university of groningen / faculty of science and engineering / zernike instute of advanced materials

Synthesis of PS-b-PAA diblock copolymer for antifouling zipper brush coatings

Ilan Ruhof (s3858774)
Prof. Dr. Marleen Kamperman, Prof. Dr. Katja Loos

Master thesis chemistry,
Track: green chemistry and catalysis,
University of Groningen
August 2020 – March 2021

Abstract

Fouling is the unwanted adhesion of material to a surface and it presents an issue in many different industries. An antifouling coating prevents this adhesion and for example, brush polymers are very effective in achieving this. An innovation led to a new brush polymer, named a “zipper brush”. A zipper brush is built up by two diblock copolymers, one being partially hydrophobic and negatively charged, and the other being positively charged and fouling-resistant. The hydrophobic diblock copolymer is adhered to a hydrophobic surface. The adhesion makes the zipper brush easy to apply and repair. To research the properties of this polymer brush coating, a flexible synthesis method to obtain different ratios and lengths is required. These varying ratios are investigated in order to optimize the first layer of the zipper brush and subsequently improve the antifouling properties.

In this project, a method to synthesize a diblock copolymer consisting of a hydrophobic polystyrene (PS) block and a hydrophilic poly(acrylic acid) (PAA) block via reversible addition−fragmentation chain-transfer (RAFT) polymerization was successfully developed. The first RAFT polymerization synthesis of PS with DDMAT as a chain transfer agent (CTA) was monitored by NMR and obtained polymers were analysed by GPC. A second block of poly(tert-butyl acrylate)(PtBA) was added by RAFT, again monitored by NMR and measured by GPC. The PS-*b*-PtBA polymer was then deprotected with acid (HCl) in 1,1,1,3,3,3-hexafluoro-2-propanol (HFIP), resulting in a fully deprotected PS-*b*-PAA polymer. Various ratios and lengths of PS-*b*-PAA diblock copolymer with low dispersity (PDI <1.3) were synthesized reproducibly. A CTA removal was performed on PS-*b*-PAA to investigate the influence of the CTA on brush formation. This was assessed by analysing the micelle formation of the diblock copolymer. Using a photocatalytic reaction, the CTA was successfully removed from the PS-*b*-PAA diblock copolymer.

1 Contents

1.1 List of abbreviations

PS	-	Polystyrene
tBA	-	Tert-butyl acrylate
PtBA	-	Poly(tert-butyl acrylate)
PAA	-	Poly(acrylic acid)
RAFT	-	Reversible addition-fragmentation chain-transfer
CTA	-	Chain-transfer agent
AIBN	-	Azobisisobutyronitril
DDMAT	-	2-(Dodecylthiocarbonothioylthio)-2-methylpropionic acid
PR3	-	Tri-n-butylphosphine
NH2R	-	Hexylamine
$CDCl_3$	-	Deuterated chloroform
DMSO	-	Dimethyl sulfoxide
MeOH	-	Methanol
THF	-	Tetrahydrofuran
DMF	-	Dimethylformamide
HFIP	-	1,1,1,3,3,3-hexafluoro-2-propanol
TFA	-	Trifluoroacetic acid
DCM	-	Dichloromethane
PDI	-	Polydispersity index
NMR	-	Nuclear magnetic resonance
GPC	-	Gel permeation chromatography
DLS	-	Dynamic light scattering

2 Theory

2.1 Background

Fouling is a process where materials from the environment, like microorganism, particles, or macromolecules, unwantedly attach to a surface[1]. This undesirable process is a hinder in many applications like marine, medical, or industrial settings. Foulants in medical applications can lead to implant rejections, malfunctioning biosensors, or the spread of infectious diseases, all of which impose a danger to health. For an industrial setting, foulants can cause problems like water contamination, pipe blockage, or increased energy consumption[2]. For marine environments when foulants attach to the hull of a ship, it can lead to increased drag, engine stress, corrosion, and fuel consumption[3]. Up to 150 billion dollars could be saved annually if the global maritime industry could make use of effective fouling protection[3].

Antifouling coatings are layers of material that can be applied to a surface to prevent foulants from adhering to it. For many years, there has been an effort to discover new approaches and techniques for fouling resistant coatings, which is driven by the need for more sustainable and eco-friendly alternatives. Early antifouling coatings were mainly designed to be antimicrobial and were mainly focused on killing those foulants. The very first systems varied from copper or lead metal sheets attached to the bottom of a vessel, to full antimicrobial coatings containing arsenic, mercury, and copper that were applied to the ship's hull. These coatings functioned well for their intended purpose but lacked lifetime effectiveness, as it only proved to be effective for a maximum of 2 years. To improve on this flaw, industry introduced biocidal tributyltin (TBT) into the coatings, which extended its lifetime up to 5 years. Unfortunately, the widespread use of these metal-based antifouling coatings led to contamination and destruction of ecosystems[4]. After this was reported, a global ban on these types of metal-based antifouling coatings was introduced.

2.2 Incentives

The development of nontoxic, eco-friendly alternatives was stimulated as a result of this ban. For example, fouling-release coatings that included polymers (e.g. silicones, fluoropolymers), waxes, oils, or natural coatings containing harvested antifouling component from organisms, started to appear on the market[5]. However, these new coatings had a drawback in commercialisation. The components needed were only available in limited supply, they had short-term effectiveness, they were expensive, or it required very specific natural antifouling ingredients. Besides the drawbacks in commercialisation, many of the coatings had issues meeting the newly established requirements for antifouling coatings.

The industry shifted towards polymer-based coatings, as these more easily met the requirements set by the environmental legislation. Polymers are cheap, biocompatible, highly versatile, nontoxic, and are easy to process. These materials lead to numerous options in the design of an antifouling coating. By modifying the architecture and functionality of the polymers, the interfacial properties can be fine-tuned, including the antifouling behaviour. These modifications can be categorised as antifouling strategies.

2.3 Antifouling strategies

The fouling adhesion process mainly depends on the surface properties. Modifying the surface properties, like surface energy, wettability, and microtexture provides a straightforward method to fouling control. Therefore, by treating a substrate with a layer of antifouling coating, the desired modification can be achieved. However, there exists a wide variety of different types of foulants, which bind in different ways. This creates a need for different approaches to design the antifouling coating. There are different antifouling coating strategies that can be used, namely: fouling-resistant, fouling-release, and fouling-degrading coatings[5].

The first type is fouling-resistant coatings, which prevents the adhesion of proteins, algae, or bacteria. This effect usually arises from the formation of a strongly hydrated surface, because this creates a barrier to foulants due to a free energy and physical barrier.

The second type is fouling-release coatings, which allow a weakly bound adhesion of foulants to the coating. However, by applying a mechanical force or limited shear, these foulants can be released again, removing them from the surface.

The third type is fouling-degrading coatings, which try to destroy the foulant itself. This is achieved either by degrading absorbed organic material with oxidizing agents, or through bactericidal functionalities that remove bacteria or other microorganisms.

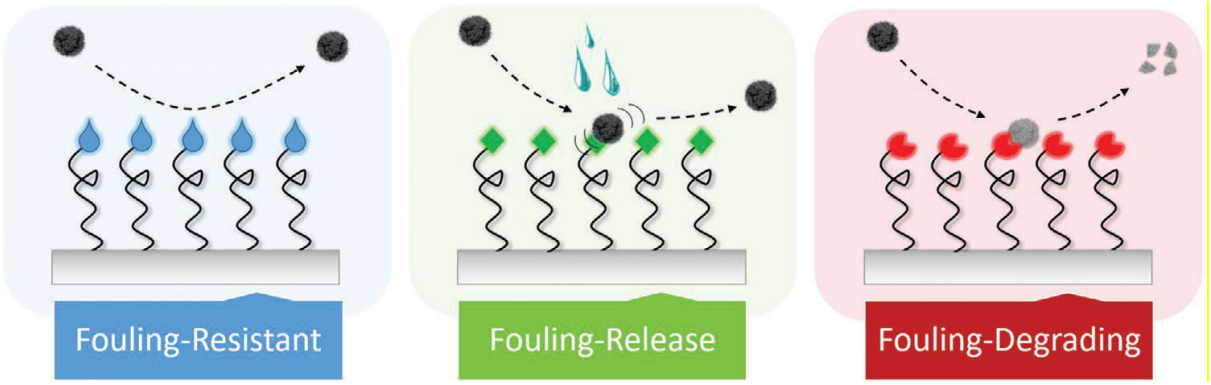

Figure 1 The three different anti-fouling strategies that can be utilised in anti-fouling coatings to prevent foulants from adhering. The picture is reproduced from Maan et al, reference 1.

Figure 1 illustrates these three strategies. The three mentioned antifouling strategies have been realised through several means, like the modification of the surface chemistry, surface topography, and architecture. The first two of these focus on the surface characteristics and the last one on the coating interior.

2.3.1 Surface chemistry

Fouling surface chemistry is all about the interaction between the foulant and the surface. It allows the coatings to be any of the three types depicted in Figure 2. An example of a fouling-release coatings would be a hydrophobic coating, which grants the surface a self-cleaning effect. In the case of a fouling-degrading coating, this can be achieved by integrating a biocidal moiety, which will kill microorganisms upon settlement. And lastly, to demonstrate fouling-resistant coatings, the surface is often hydrophilic, electrically neutral, and hydrogen bond-forming. This forms a free energy and physical barrier due to a tightly-bound water layer.

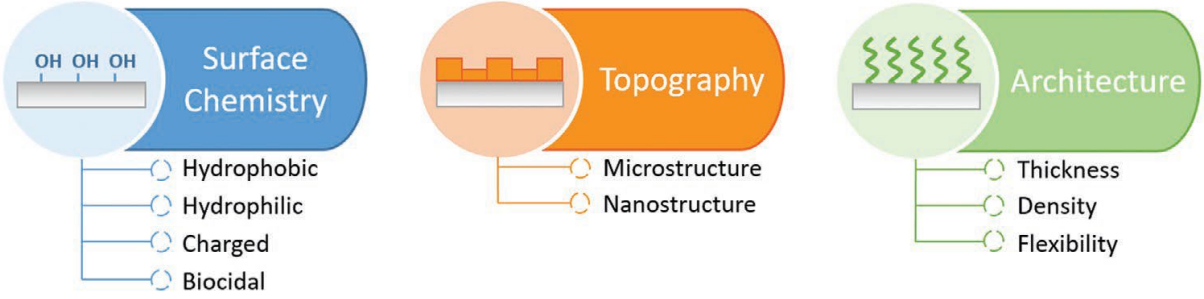

Figure 2. The three approaches to augment a surface with antifouling properties, with examples of changeable parameters. The picture is reproduced from Maan et al, reference 1.

Surface topography is about the actual volume of the coating. The ideal circumstances for microorganisms to adhere would be a cavity that is slightly larger than themselves. This provides the most protection and surface area contact. By changing the topography of the surface, the amount of suitable cavities can be restricted. This either prevents adhesion all together, or allows for easy removal of foulants after adhesion. As a result, both fouling-resistant and fouling-release types of coatings can be designed with the approach.

The architecture of the coating is not focused on the surface, but rather on the interior of the layer itself. Polymer brushes are an example of structured soft matter coatings, in which architecture is important. A polymer brush[7,8] is defined as: "a densely packed array of polymer chains, end-attached to an interface and stretched out into solution[1]." To visualise this, imagine a patch of seaweed in the ocean. These grow as an array underwater, while attached to the seafloor. This shape is replicated on a molecular scale in case of a polymer brush. Foulants can adhere in three ways to these types of coatings:

1. Primary adsorption, in which a foulant goes through the layer and adheres onto the substrate itself.
2. Secondary adsorption, in which a foulant is adsorbed on top of the polymer brush.
3. Tertiary adsorption, in which a foulant is adsorbed inside the polymer brush itself.

The architecture of a polymer brush presents its form, like linear brushes, cyclic brushes, or bottle brushes. Changing the architecture can alter the surface coverage, enable the formation of a structured surface, or limit the foulant-surface interaction. The grafting density is a parameter to define the distance between each polymer chain from each other, and is important to take into account when developing such coatings.

2.3.2 Polymer brushes

This polymer brush coating structure brings a distinct advantage for antifouling applications. A polymer brush introduces a physical barrier between the surface and the approaching foulant. If the foulant would try and adhere, the polymer brush would need to compress. This compression is entropically unfavourable and would reduce the total number of conformations, leading to steric repulsion and preventing the adsorption of the foulant. A polymer brush can also tightly bind a hydration layer that surrounds the brushes. In this case, water would have to be moved to make space for the approaching foulant. This leads to the repulsion of the foulant, as the dehydration process is thermodynamically unfavourable. To summarize, due to the interesting characteristics of these polymer brushes, their antifouling possibilities seem very achievable.

A recent in-depth review[1] about possible antifouling polymer coatings lists and details all the various possibilities on this subject. Mentioned in the review are polymer brushes, which are the subject of this research. Polymer brushes are one of the more widely researched antifouling coating systems. This is because polymer brushes are an excellent component for coatings to change the antifouling behaviour, as an extremely thin layer can already drastically transform the surface properties[5]. For example, a nanometer thick layer can change the surface in hydrophobicity or charge.

2.4 Zipper brush polymers

By combining strategies together, it becomes possible for them to synergise. The specific pairing of fouling-resistant and fouling-release coatings is the cornerstone for the design of the zipper brush polymers made by de Vos[6,9] et al.. A zipper brush is built up by two polymers with one negatively charged, and the other being a diblock copolymer which is positively charged and fouling-resistant. As shown in Figure 3, the negatively charged red chain connected to the surface binds with the positively charged green chain that is part of a diblock copolymer. The black chain is a fouling-resistant polymer block that prevents adhesion. Since the grafting density is determined by charge compensation, a smaller positively charged chain leads to a higher grafting density, as more chains need to be attached to compensate the negative charges already present on the surface. The fouling-resistant properties are integrated in the black chain and it is supported by a foulant-release mechanism through the charged blocks. When a foulant finds a way to adhere to the uncharged chain, it can still be possible to easily remove the foulant by changing the charge compensation by for example pH or salt concentration. This would consequently release the diblock copolymer and attached foulant. This leads to an easy removal of foulants and the simple repair of the zipper brush. This is a synergistic strategy combining both foulant-release and fouling-resistance.

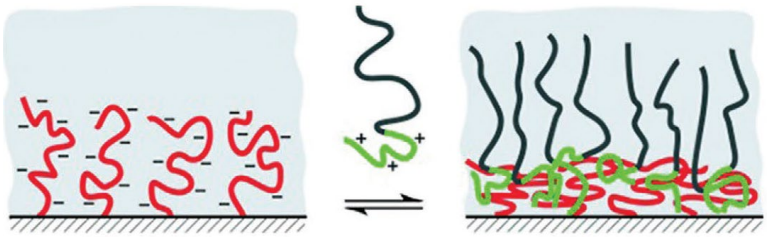

Figure 3 The depiction of a zipper brush. The red chains are charged and attached to the surface. The positively charged green chains then seen charge compensation and adhere to the red chains. The black chains are uncharged and fouling-resistant. This picture is reproduced from de Vos et al, reference 6.

Conventional polymer brushes are covalently bound to the surface, which leads to a rigid and smooth layer. However, for certain applications as in maritime industry, the costs of applying such coatings would be too high to be considered viable/feasible. In the ideal situation, the coating could be applied directly to a ship floating in water. To achieve this, it is possible to apply a coating through adhesion, which does not covalently bind to the surface. The coating would be easy to apply, but would be less strongly attached to the ship's hull. So instead of covalently binding the first charged polymer brush to the surface, it is done through adhesion. This forms a zipper brush as well, but can easily be applied to a surface. The advantages of an adhered zipper brush are the easy application and repair of both types of diblock copolymers. The grafting density of the first adhered diblock copolymer can be influenced by changing the ratio of the lengths of the blocks. A longer uncharged adhering block leads to a lower grafting density as the chains will be positioned further apart, and vice versa.

Another currently ongoing research into the viability/feasibility of these zipper brush coatings is requiring the synthesis of these polymer brush components. The specific polymer that was required is a diblock copolymer made from a polystyrene (PS) block and a poly(acrylic acid) (PAA) block.

2.5 Objective

In this thesis, the synthesis of a polystyrene-*b*-poly(acrylic acid) (PS-*b*-PAA) diblock copolymer is reported. This polymer is the first part of a zipper brush polymer currently being studied. The composition of the polymer directly relates to the antifouling coating properties, requiring good control during synthesis. The goal of each synthesis was to produce a specific polymer block ratio, while maintaining a narrow polydispersity index. A repeatable, simple, and effective procedure of the synthesis of a PS-*b*-PAA diblock copolymer with a specific block ratio and block length is reported in this thesis.

2.6 RAFT

The grafting density heavily influences the properties of the zipper brush, and therefore requires a diblock copolymer synthesis technique that allows for strict control over the length of both blocks. One such polymerisation technique is RAFT polymerisation. Reversible addition-fragmentation chain-transfer (RAFT) is a type of polymerisation in which a chain-transfer agent (CTA) mediates a normal radical polymerisation[10]. The same steps as with conventional radical polymerisation occur, namely: initiation, propagation, and termination. However, there are extra steps added concerning the CTA. All the following steps are also displayed in Scheme 1:

1. The first step is initiation. The reaction is started using a free-radical source. Azobisisobutyronitril (AIBN) is a conventional source and is classified as a decomposing radical initiator. The initiator decomposes into two fragments $(I\cdot)_2$ which can subsequently react with a monomer to initiate chain growth.
2. The second step is propagation. During this phase, a growing polymer chain will react with more monomer molecules to create longer chains.
3. The third step is where the RAFT agent steps in. The growing polymer chain can react with the RAFT agent and form an equilibrium. The formed RAFT adduct radical can now choose to fragment in either direction. The resulting leaving group once again forms a new radical.
4. The fourth step is the re-initiation of chain growth. The radical on the leaving group reacts with monomer and starts another active polymer chain.

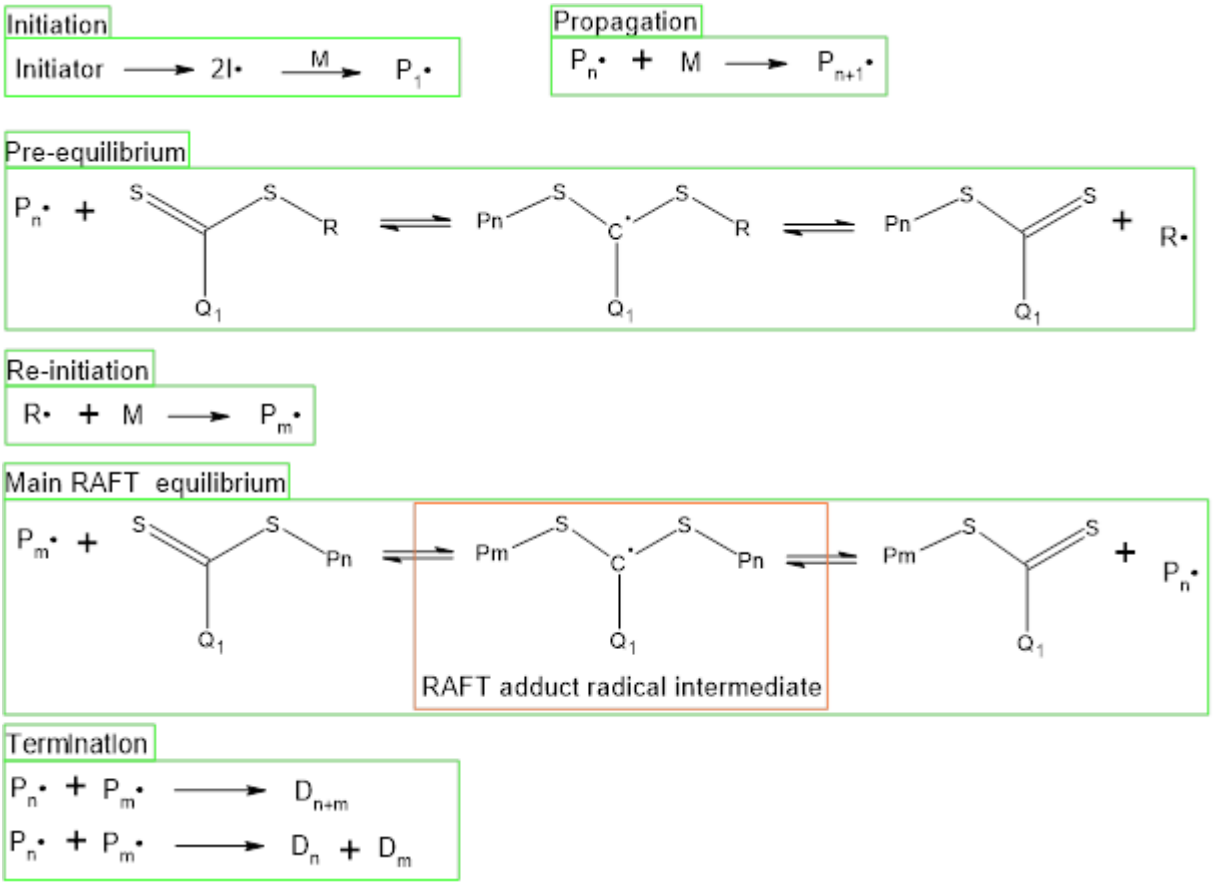

Scheme 1 An overview of conventional RAFT polymerisation phases.

5. The fifth step is the main equilibrium of the RAFT polymerisation. Here, the chains rapidly interchange between each other and are statistically given an equal chance of chain growth. This equal opportunity can often lead to a narrow dispersity.
6. The last step is the termination step. This can occur occasionally when two radical chains meet and form a dead polymer (D), which cannot react further. If the adduct radical of the CTA is sufficiently hindered, it should not undergo termination.

2.6.1 RAFT thermodynamics

The thermodynamics of the main RAFT equilibrium can have an impact on the monomer conversion rate. The relative stability between the adduct radical of the CTA and the active species for chain growth is of great importance. If the adduct radical is more thermodynamically favoured, it will mean that there are less active species present, slowing down the polymerisation process. In that case, the RAFT polymerisation is rate-retarded compared to the conventional radical polymerisation without a CTA present because of the decreased concentration of active chains [P·]. On the other hand, this limits termination, which is beneficial. This is because the rate of termination is proportional to the square of concentration of active species $[P\cdot]^2$, while the rate of propagation becomes proportional to the concentration of active species [P·]. Therefore, the rate of termination is drastically more suppressed than the rate of chain growth. The influence of both temperature and chemical factors affect this rate-retardation. A higher temperature favours fragmentation over the adduct radical. Chemical factors like radical stabilising groups (e.g. phenyl groups) on the CTA favour the adduct radical, while radical stabilising groups on the monomer favour fragmentation.

2.6.2 Advantages of RAFT

The pre-equilibrium and re-initiation steps occur very early in the polymerisation. This means that the chains all start growing at approximately the same time. Usually the number of radicals that are delivered to the system by the initiator are rather low compared to the number of CTA molecules, resulting in the majority of the chains coming from the R-group in the re-initiation step. This is important to know, since the initiator decomposes at all times during the reaction, which would result in new chains growing. Any chains that start later in the polymerisation would therefore be shorter, leading to a wide polydispersity. However, the vast majority of the chains have their origin at the CTA and do not contain the initiator molecule. This means that all chains start growing at approximately the same time, resulting in a narrow polydispersity.

Once the desired polymer length has been reached, the reaction is quenched by cooling it down and exposed to oxygen, as oxygen can react with the radical in a termination process. The formed polymer with the desired chain length is now ‘stored’ in between the R group and the di- or tri- thiocarbonate moiety of the CTA molecule. The reason for the term “stored” is because the polymerisation process is able to be restarted with the addition of an initiator that brings radicals into the system. This is also why RAFT synthesis is called ‘reversible’. If another type of monomer is introduced along with some initiator, then a block copolymer can be formed.

2.6.3 Disadvantages of RAFT

Unfortunately, there are also potential downsides to RAFT polymerisation. The CTAs are usually only suited for a certain limited set of monomers, which can quickly lead to a multistep synthesis and purification. Moreover, they can bring discolouration, can be unstable over a long time, and the di-/tri-thioester moiety can form small sulphur compounds during decomposition which can have a pungent odour. Luckily, there exist chemical purification steps that can remove these groups from a finished polymer, in case the CTA group poses an issue. This will be described in section 2.7.

To summarise, RAFT polymerisation is a highly effective technique. The benefits are a high control over the length, polydispersity index, and structure of the polymer in a wide range of solvents.

2.6.4 PS-*b*-PAA synthesis

The synthesis for PS-*b*-PAA has been done before. Diblock copolymers containing both PS and PAA segments have been successfully synthesised using atom transfer radical polymerization (ATRP)[11–14], RAFT[15–22], and nitroxide-mediated radical polymerization (NMRP)[23]. RAFT was specifically chosen due to the advantages discussed before and the availability of the reactants. While ATRP and NMRP are both viable options for the synthesis of the PS-*b*-PAA diblock copolymer, the advantages of RAFT make it the preferred and chosen synthesis method.

2.7 Micelles and CTA removal

To explain the need for a CTA removal in this research, first a phenomena called micellization needs to be defined. A micelle is an aggregate of surfactant molecules dispersed in a liquid, which form a colloidal suspension[24]. Surfactants are molecules that lower surface tension, by having one part that prefers one phase and the other part preferring the second phase. For example, in the case of an AB diblock copolymer, one part may be hydrophilic, while the other is hydrophobic. If this polymer is subsequently suspended in water, it could form a spherical micelle with its neighbouring molecules The hydrophobic part will try to reduce the volume to make the surface area as small as possible and the hydrophilic part will extend into the water phase.

If an extra block is added, thereby forming an ABA triblock copolymer, the shape of the micelle will be different. If the “A” block is hydrophobic and “B” block is hydrophilic, then the polymer can fold in on itself where both “A” blocks will aggregate. The “B” block will then form a loop instead of an arm. This type of micelle is called a flower-like micelle, as the micellar shape resembles a flower petal and aggregates of multiple micelles resemble a flower.

Once a RAFT polymer synthesis is finished, the CTA is still attached to the polymer. In many applications, this does not present an issue, as it is a very small fraction of the total polymer length. However, in case it introduces unintended side-effects or unwanted properties, it might be beneficial to remove the CTA group from the polymer. It was theorised that the CTA is giving an AB diblock copolymer, an ABA triblock copolymer character. Figure 4 illustrates how the hydrophobic CTA is similar to a hydrophobic PS block and how it mimics the triblock shape.

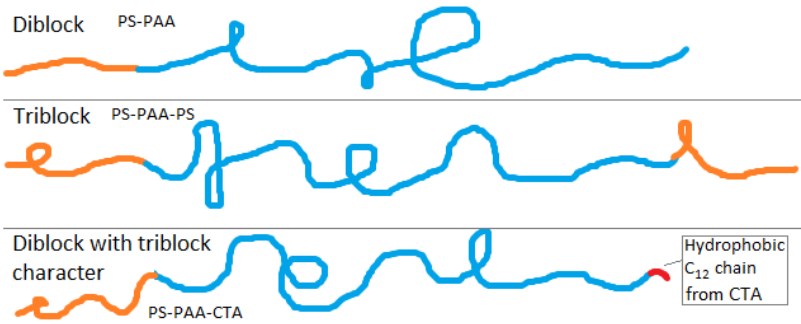

Figure 4 An illustration to demonstrate how the CTA can give a triblock character to the diblock polymer. The hydrophobic CTA can mimic the same function as the hydrophobic PS in the triblock.

This could result in the formation of unintended flower-like micelles that may hinder the formation of a functional polymer brush layer. Therefore, it could be interesting to remove the CTA from the polymer. There are multiple different approaches to remove the CTA form a RAFT-synthesised polymer[25]. An overview is given in the Figure 5 from Keddie[26] et al.

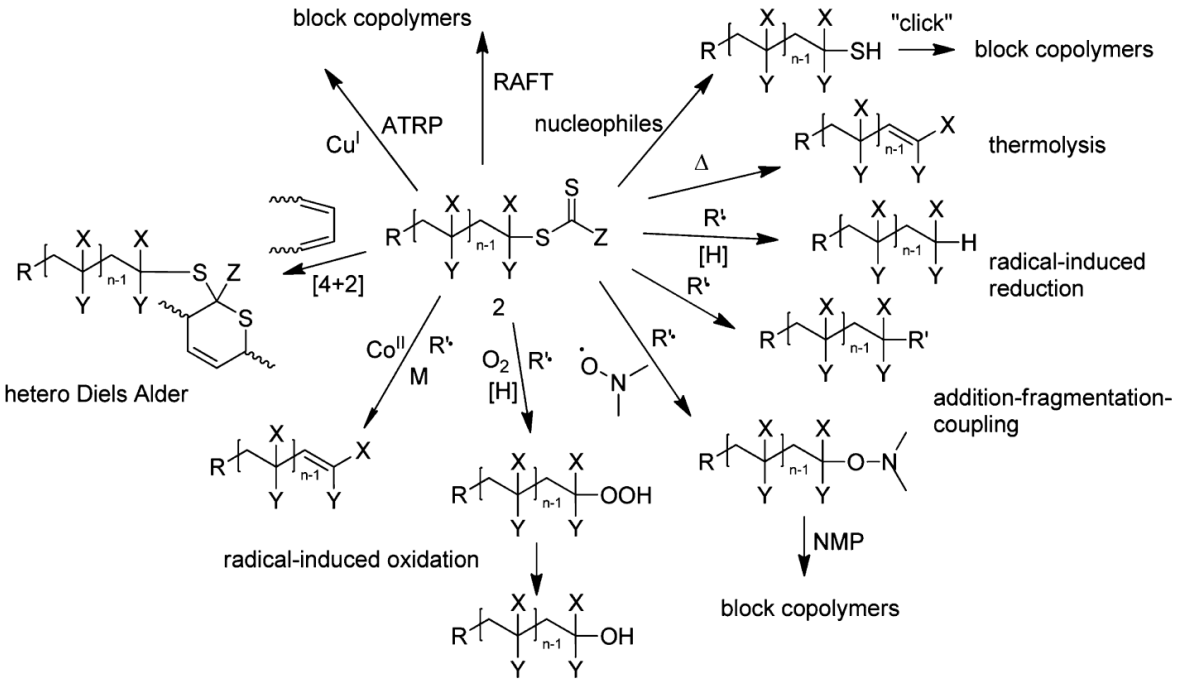

Figure 5 Various options to remove the CTA from the RAFT synthesised polymer. The picture is reproduced from Keddie et al, reference 26.

In this research, only some of the options given in Figure 5 are worth trying, focusing mostly on the options that remove the CTA end group entirely. One of these options could be thermolysis, which means that the polymer is heated to a high temperature in order to remove the CTA. However, this is problematic as it can lead to polymer degradation. Therefore, instead of a physical approach, a chemical approach is preferred. The ideal case would be that the end group is removed without introducing a new functionality.

Radical-induced reduction is one way to achieve complete removal of the CTA and has been studied by several researches[26–31]. By activating the polymer chain growth step and letting it react with a hydrogen donor, it can terminate the chain growth leading to CTA removal. The main issue is that it may cause addition-fragmentation-coupling, which is a termination occurring when two radical polymer chains meet each other. This unwanted termination leads to the formation of an ABBA triblock copolymer and it will double the chain length. Therefore, the reaction conditions must mediate the formation of radicals and prevent unwanted termination reactions.

An article by Discekici[32] et al. showed the photocatalytic removal of the thio moiety that is present in RAFT agents. A reaction mechanism was proposed by Discekici et al and is displayed in Scheme 2. Firstly, the tri-thio moiety reacts with an amine. The second step is the reaction between the thiol group on the polymer and the excited state of the photocatalyst. This creates a radical ion on both the photocatalyst and the thiol group. The thiol then loses a hydrogen to form a sulphur radical. The third step is the reaction with a phosphine group.

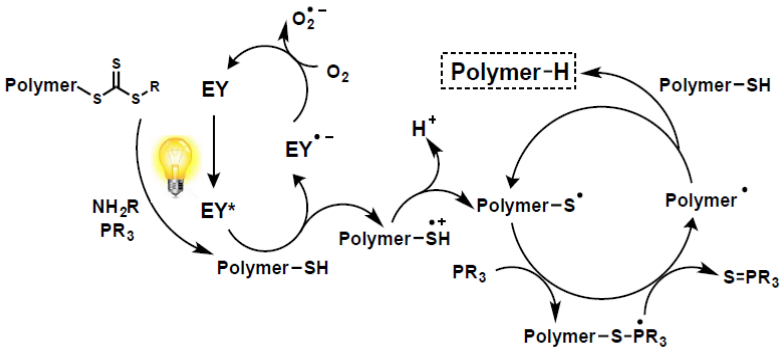

Scheme 2 The proposed mechanism of photocatalytic CTA removal by Discekici. The image is reproduced from Discekici et al, reference 32.

The high reactivity of phosphine groups can quickly lead to the reaction between phosphine and sulphur, removing the sulphur entirely. The radical is left on the polymer chain, which reacts with a hydrogen on an unreacted thiol group. The reactivity of the phosphine is the primary reason why chain doubling termination reactions are not reported, as it will quickly react with the radical before anything else.

2.8 Approach

The synthesis route for the synthesis of polystyrene-*b*-poly(acrylic acid) (PS-*b*-PAA) is shown in Scheme 3. It involves the follow steps:

1. RAFT polymerisation of PS-CTA
2. RAFT polymerisation of PS-*b*-PtBA
3. Deprotection of PS-b-PtBA to PS-*b*-PAA
4. Optional CTA removal step

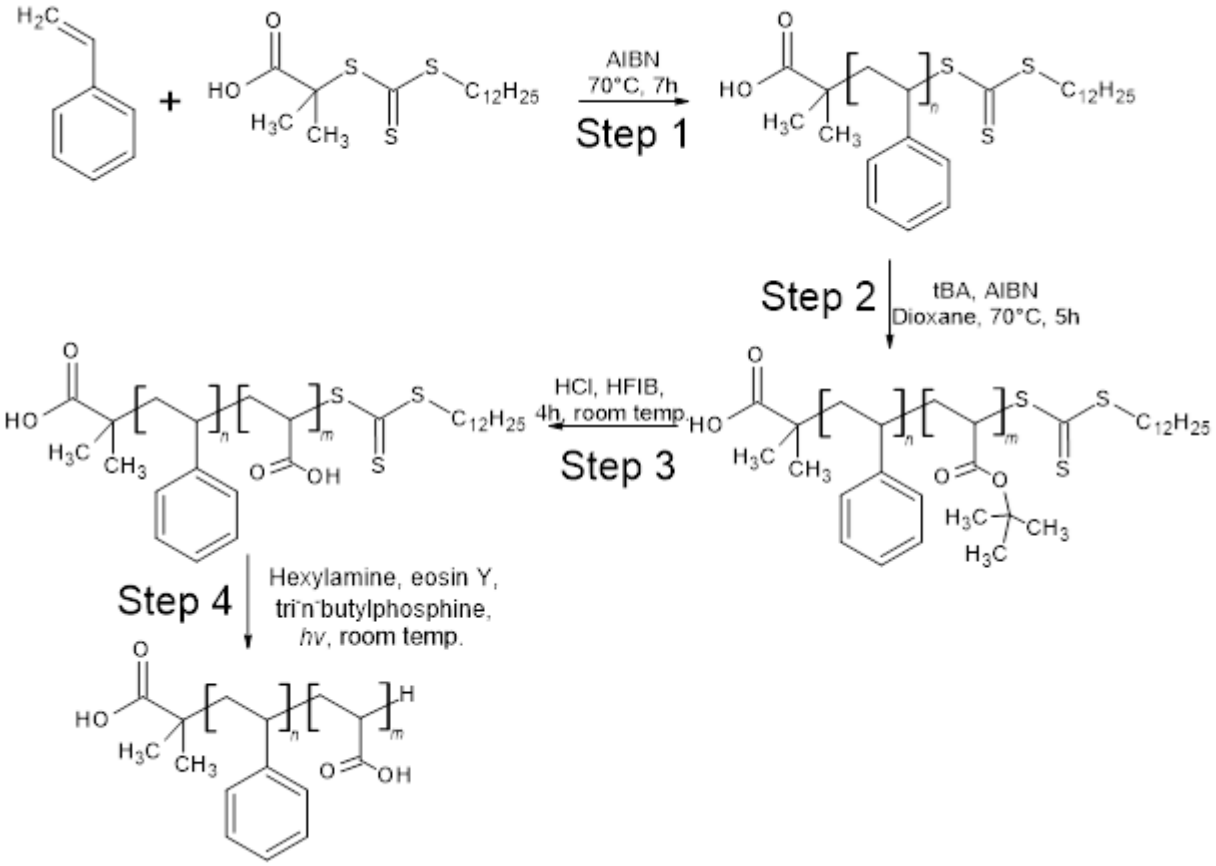

Scheme 3 An overview of the total synthesis route of PS-b-PAA.

The synthesis started with the RAFT polymerisation of styrene, using 2-(Dodecylthiocarbonothioylthio)-2-methylpropionic acid (DDMAT) as a chain transfer agent (CTA) and AIBN as a radical initiator. After the reaction, polystyrene is obtained through precipitation and was analysed by NMR and GPC. This PS-CTA was used for the next step, with the goal of adding the second block. This involved growing a block of tert-butyl acrylate (tBA) between the polystyrene and the chain transfer agent. By reacting the PS-CTA with tBA, in a solvent containing AIBN, the diblock copolymer PS-*b*-PtBA was made. This polymer was precipitated and analysed on NMR and GPC.

The last step involved the deprotection to remove the tert-butyl moiety. This is conventionally done by using acid in dichloromethane, but a recently found alternate method demonstrated a more efficient and shorter reaction step. The PS-*b*-PtBA diblock copolymer was reacted inside hexafluoro-2-propanol (HFIP) solvent containing HCl as the acid. The resulting PS-*b*-PAA polymer was precipitated and analysed by NMR. This polymer was not analysed by the GPC as most of the chain is charged, which would result in destroying the GPC column. Although, this is not an issue as the deprotection step does not change the total length of the polymer.

Due to complications observed when applying the formed diblock copolymer, another step was performed. As mentioned previously, it was theorised that the DDMAT chain transfer agent (CTA) was changing the diblock character into a triblock character, leading into more complex micelles being formed. The optional step was included to remove the CTA from the diblock copolymer using a photocatalyst. The intention behind the step is to completely remove the tri-thio moiety of the DDMAT including the alkyl (C_{12}) connected to it. This was done by reacting the CTA containing polymer with an amine, phosphine, and photocatalyst.

3 Materials and methods

3.1 Materials

Styrene (Sigma-Aldrich, 99%, stabilized with 4-tert-butylcatechol) was purified by SilicaFlash P60 (Silicycle, 40-63 µm) column. Tert-butyl acrylate (tBA, Sigma-Aldrich, 98%, with 10-20 ppm monomethyl ether hydroquinone as inhibitor) was purified by SilicaFlash P60 (Silicycle, 40-63 µm) column. Deuterated chloroform ($CDCl_3$, Sigma-Aldrich, 99.8%), deuterated dimethyl sulfoxide (DMSO-d^6, Sigma-Aldrich, 99.5%), DDMAT (Sigma-Aldrich, 98%), Azobisisobutyronitril (AIBN, Sigma-Aldrich, 98%), Hexylamine (Sigma-Aldrich, 99%), Tri-n-butylphosphine (Sigma-Aldrich, 93.5%), and eosin Y (Sigma-Aldrich, 99%) were all used as received. All solvents used were of analytical grade.

3.2 Characterisation

For ^{1}H nuclear magnetic resonance (^{1}H-NMR) spectra, all non-polar polymer samples (PS, PS-*b*-PtBA) were dissolved in deuterated chloroform ($CDCl_3$). The samples taken during the reactions were placed into the NMR tube directly and dissolved with 0.6ml $CDCl_3$. For the dried polymer, 10mg of sample was dissolved in 0.6ml $CDCl_3$ using a vial and once dissolved poured into a NMR tube. ^{1}H NMR spectra were recorded at 400 MHz. The chemical shifts for samples dissolved in $CDCl_3$ were recorded in ppm (δ) and measured from -1 to 12 ppm. All polar polymer samples (PS-*b*-PAA) were dissolved in deuterated dimethyl sulfoxide (DMSO-d_6). The samples taken during the reactions were placed into the NMR tube directly and dissolved with 0.6ml DMSO-d_6. For the dried polymer, 10mg of sample was dissolved in 0.6ml DMSO-d_6 using a vial and once dissolved poured into a NMR tube. The chemical shifts for samples dissolved in DMSO-d_6 were recorded in ppm (δ) and measured from -1 to 14 ppm. The obtained spectra were analysed and integrated using MestReNova software, version 14.1.2.

Size exclusion chromatography (SEC) was performed on a Viscotek GPCmax system equipped with a TDA 302 triple detector array (both Malvern). PolarGel L and PolarGel M columns (Agilent, 8 µm 30 cm) were fitted into the machine and kept at a temperature of 50 °C. N,N-dimethylformamide (DMF, 99.9 %, Sigma-Aldrich) with 0.01 M LiBr was used as eluent. Samples were dissolved in the eluent at a concentration of ≈2mg/mL and passed through a 0.45 µm nylon filter prior injection. Near monodisperse standards (Polymer Standard Services) were used for the construction of a calibration curve. Data acquisition and calculations were performed using Viscotek OmniSec software version 5.0, in addition to being exported to excel.

The dynamic light scattering (DLS) measurements were done on a Malvern Zetasizer Ultra. The UV/VIS measurements were done using a Analytik jena Specord 210 plus, with quartz cuvets.

3.3 Raft polymerisation synthesis of PS

To start the polystyrene synthesis, DDMAT (39.9 mg, 109 µmol), AIBN (2 mg, 12 µmol) with a 1:9 ratio to DDMAT, Styrene (1.16 g, 11.1 mmol), were charged into a round-bottom flask equipped with a stir bar and rubber septum. The reaction mixture was bubbled with nitrogen for 10 min before immersing the flask into a preheated 70°C oil bath. After 7 hours at 70°C, the flask was cooled to room temperature and opened to air. Any samples taken during the reaction were performed under a nitrogen flow, using a nitrogen purged needle and syringe to prevent oxygen from entering the reaction environment. The polymer was precipitated into MeOH twice to remove impurities and unreacted monomer. Each precipitation step included a 5-minute centrifuge step at 4500 rpm to force to the polymer to precipitate. The polymer was dried overnight in a vacuum oven at 40°C before analysing by NMR and GPC.

3.4 Raft polymerisation synthesis PS to PS-*b*-PtBA

For the diblock copolymer synthesis, PS (150 mg, 44 µmol), AIBN (0.8 mg, 5 µmol) with a 1:9 ratio to DDMAT present in the PS, tert-butyl acrylate (3 g, 23.4 mmol), and DMF (10 ml) were charged into a 25mL round-bottom flask equipped with a stir bar and rubber septum. The reaction mixture was bubbled with nitrogen for 10 min before immersing the flask into a preheated 70°C oil bath. After 6 hours at 70°C, the flask was cooled to room temperature and opened to air. Any samples taken during the reaction were performed under a nitrogen flow, using a nitrogen purged needle and syringe to prevent oxygen from entering the reaction environment. The polymer was dissolved into MeOH and precipitated in demineralised water twice. Each precipitation step included a 5-minute centrifuge step at 4500 rpm to force to the polymer to precipitate. The polymer was dried overnight before analysing by NMR and GPC

3.5 Deprotection of PS-*b*-PtBA to PS-*b*-PAA

The deprotection was conducted by following a literature procedure by Filippov et al.[33]. To perform the deprotection synthesis, PS-*b*-PtBA (100 mg, 2.8 µmol), a 1.3 excess ratio of HCl (81 µl, 0.97 mmol), and HFIP (30 ml) were charged into a 50mL round-bottom flask equipped with a stir bar and rubber septum. The reaction mixture was left stirring at room temperature for 4 hours. Afterwards, the volatiles were removed in vacuo and the dry polymer was dissolved in THF followed by a precipitation in n-pentane. The precipitation step included a 5-minute centrifuge step at 4500 rpm to force to the polymer to precipitate. The polymer was dried overnight in a vacuum oven at 40°C before analysing by NMR.

3.6 CTA removal from PS-CTA to PS-H

A 25ml round-bottom flask equipped with a magnetic stir bar and a rubber septum was placed under a nitrogen atmosphere. In the flask, PS (60 mg, 0.017 mmol) was added and dissolved in 1ml DCM. Once dissolved, hexylamine (27.44 µl, 0.209 mmol) and eosin Y (0.602 mg, 0.9 µmol) were added after making an appropriate stock solution. Following this, tri-*n*-butylphosphine (12.88 µl, 0.052 mmol) was added after making an appropriate stock solution in a separate nitrogen environment. The vial was degassed with nitrogen for 10 minutes and irradiated with blue LEDs for 24 hours. The polymer was dissolved in methanol and precipitated in water twice. Each precipitation step included a 5-minute centrifuge step at 4500 rpm to force to the polymer to precipitate. The polymer was dried overnight in a vacuum oven at 40°C before analysing by NMR and GPC.

3.7 CTA removal synthesis of PS-*b*-PtBA-CTA to PS-*b*-PtBA-H

A 25ml round-bottom flask equipped with a magnetic stir bar and a rubber septum was placed under a nitrogen atmosphere. In the flask, PS-*b*-PtBA (500 mg, 0.011 mmol) was added and dissolved in 1ml DCM. Once dissolved, hexylamine (17.92 µl, 0.136 mmol) and eosin Y (0.393 mg, 0.6 µmol) was added after making an appropriate stock solution. Following this, tri-*n*-butylphosphine (8.41 µl, 0.034 mmol) was added after making an appropriate stock solution in a separate nitrogen environment. The vial was degassed with nitrogen for 10 minutes and irradiated with blue LEDs for 24 hours. The polymer was dissolved in methanol and precipitated in water twice. Each precipitation step included a 5-minute centrifuge step at 4500 rpm to force to the polymer to precipitate. The polymer was dried overnight in a vacuum oven at 40°C before analysing by NMR and GPC. Later on, part of this was further converted to PS-*b*-PAA using the method as described at section 3.5.

4 Results and discussion

In this chapter, the results of all the syntheses and polymerisations are described and discussed. It follows the order mentioned in the approach, starting with the synthesis of PS.

4.1 RAFT polymerisation synthesis of polystyrene

The preparation of the synthesis involved researching previous methods and data. After obtaining previous experimental data, it showed that an estimated conversion of 30% could be achieved after 7 hours of reaction time. While this might seem to be a low conversion, it has to be noted that the styrene is also its own solvent, making it more efficient than it initially seems. The idea of a 'master batch' was proposed early on, which means a larger scale experiment to produce enough material to do every subsequent step with the same batch. This would prevent individual batches from influencing the results of subsequent reactions, making them more comparable with each other. This meant that the master batch needed to be as good as possible.

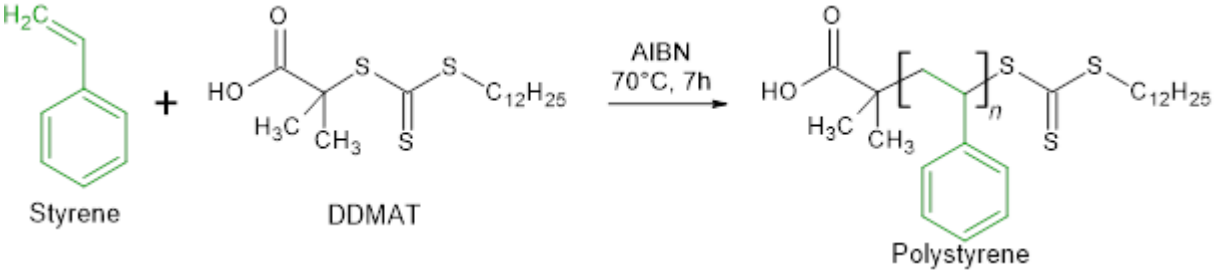

Scheme 4 shows the reaction scheme of the polystyrene RAFT synthesis.

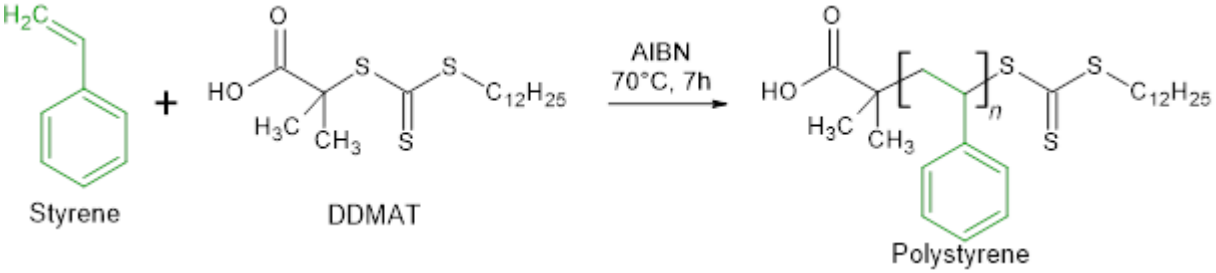

Scheme 4 Polystyrene RAFT synthesis reaction scheme

4.1.1 Polystyrene synthesis NMR calculations

The NMR data of samples taken during and/or after the reaction were integrated to calculate the conversion. An example of this type of calculation is given in this section. The used NMR spectra can be found in the Appendix (7.1.1 and 7.1.2).

For 7.1.1, which is the sample taken before the reaction but after purging, the area of both the aromatic and aliphatic regions were integrated. During N_2 purging some styrene might evaporate which is why it is more accurate to take the sample after purging. This sample was regarded as the baseline for the experiment and the following samples were compared to these values. For 7.1.2, which is the finished reaction, the aromatic and aliphatic regions were integrated. By subtracting the aromatic region with the T0 aromatic region, the hydrogens that moved here due to polymerisation can be measured, which is both the monomer and solvent correction. Due to the 5 hydrogens in the ring, the value then has to be divided by 5. The resulting value is polystyrene, which can be used to calculate the conversion by: $conv.(\%) = \frac{PS}{PS+1}$

This method does not offer the very best accuracy, but it is well within the accuracy of the NMR. It can be used to make fast decisions during synthesis and it can be used as an indication. A potential issue that can occur is the difference in solvent to sample ratio, making this not a qualitative method. The can be minimised by using the same amount of sample and solvent each time. As shown in the following section, it is reliable enough when compared to the more accurate method of GPC.

4.1.2 Polystyrene synthesis exploration

Before the synthesis of a master batch with which every subsequent reaction was done, the synthesis was first explored in terms of duration and reliability. To gain a clearer overview of the reaction, several samples were taken during the polymerisation experiment. This was done by setting a nitrogen flow in the reaction flask and taking a sample using a syringe with a nitrogen purged needle. The nitrogen atmosphere needed to be maintained to avoid any potential termination reaction involving atmospheric oxygen. Once the sample was taken, the nitrogen flow was removed by removing the outlet first to induce a nitrogen pressure. The samples were dissolved in $CDCl_3$ and left to dissolve for 10 minutes. The samples were then measured using the NMR and integrated to calculate the conversion based on peak area. This progression of conversion data for both the aromatic and aliphatic regions is plotted in Figure 6.

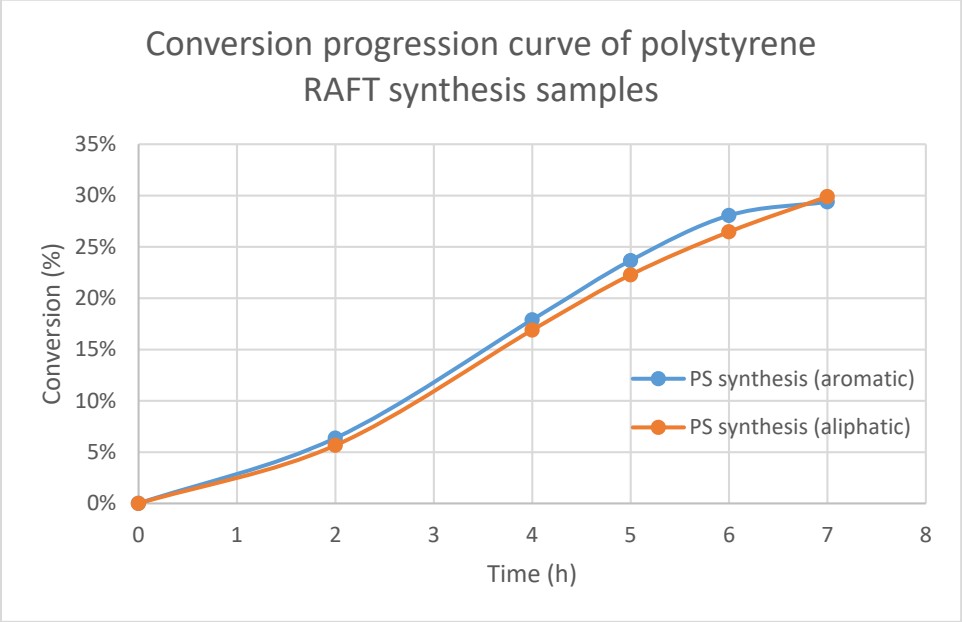

Figure 6 The progression of the conversion of polystyrene from styrene during RAFT synthesis, by comparing the aromatic region and aliphatic region with the monomer peak.

The conversion curve with the integrated NMR data in Figure 6 shows an increase in aromatic and aliphatic region compared to the monomer peaks. This is expected and is explained by an increase in polymer length by consuming monomer. As previously mentioned, the target for conversion was set at 30% after 7 hours and this target was clearly achieved. To check and gain a clearer picture, these samples were also measured using GPC. This was done to reaffirm that chain growth had taken place and to indicate the chain length growth over time. The NMR samples were dried to remove any solvent or spare monomer and were then dissolved in DMF with 0.1M LiBr. These were injected into the GPC and the results are depicted in Figure 7.

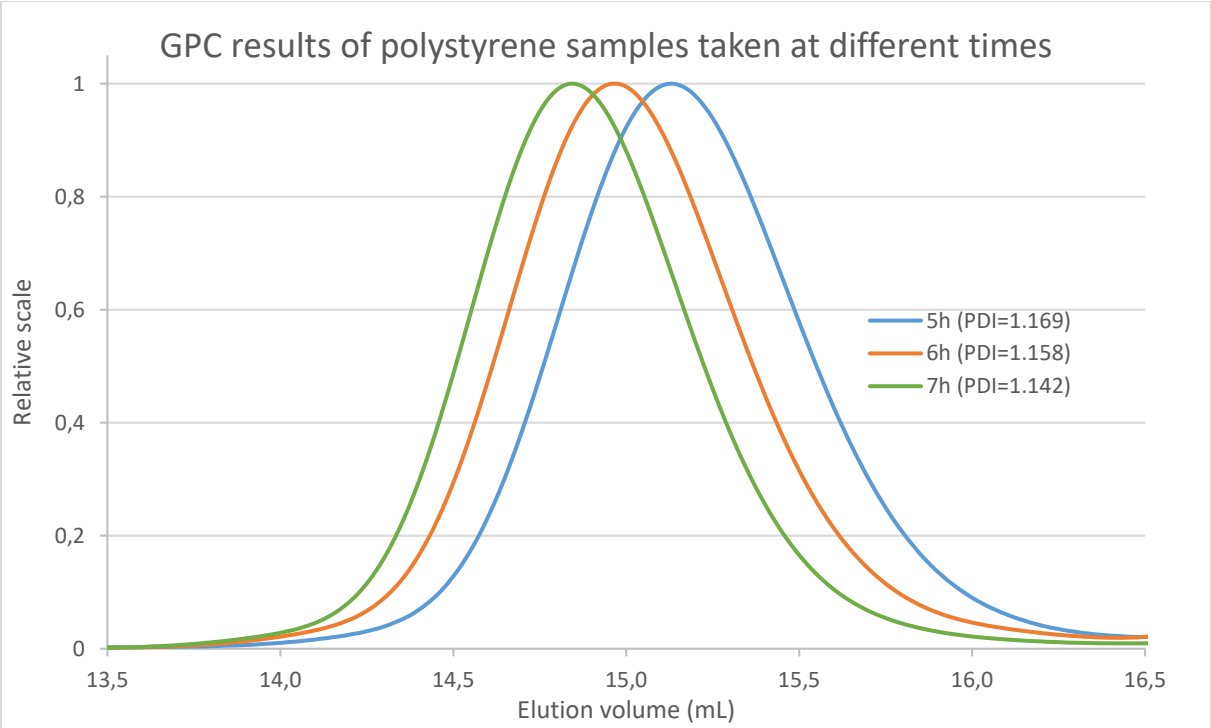

Figure 7 The GPC curve of three samples taken at different times from the same reaction. It shows three polymers with narrow dispersity and increasing chain lengths.

As shown in Figure 7, an increase in chain length is observed as each subsequent sample takes less time to elute. The dispersity of each sample is good and slowly lowers as time progresses. This can be seen by the symmetrical shape of the peaks and shows a well-controlled polymerisation. It shows that the number of chains that are longer than the average chain length, is similar to the number of chains shorter than the average chain length. By comparing the NMR and GPC directly next to each other as shown in Table 1, it is visible that there are minor differences.

Table 1 The molecular weights measured by GPC and NMR for three samples that were taken at different times during the same experiment.

	Mn (GPC)	Mw (GPC)	Mn (NMR)
5h	1941	2270	2177
6h	2335	2705	2746
7h	2707	3091	3087

The styrene monomer still present in the reaction mixture had to be removed to obtain a clean dry polymer able to be used for the next step. This was done through precipitation by pouring it into a large excess of methanol. The powder was then redissolved in preferably as little dioxane as possible, leaving it as concentrated as possible, which was then once again added to an excess of methanol. If there is a lower concentration of polymer in dioxane, some polymer will refuse to precipitate because the dioxane will keep it in solution, leading to a lowered yield. Each precipitation step included a 5-minute centrifuge step at 4500 rpm to force to the polymer to precipitate, which helped to remove most cloudiness that formed by dissolved polymer. After overnight drying under vacuum, a dried PS polymer was obtained and stored. The yield for the master batch was 72%. This was deemed adequate and was slightly lower than expected due to extra washing steps.

4.1.3 Polystyrene NMR analysis

Figure 8 shows the NMR spectrum of the RAFT synthesised polystyrene (PS_{30}) in $CDCl_3$ (7.26ppm). The NMR spectrum is divided in two major regions and there are three labelled parts in the polymer to consider. The first region is the aromatic region and it is between 6.3ppm and 7.5ppm. This is where the ring structure in styrene can be found and is labelled A. The other region is the aliphatic region, which is between 0.8ppm and 2.5ppm. This is where the hydrogens present in the backbone of the polymer can be found. The last labelled area is the peak at 3.25ppm which indicates the hydrogen next to the sulphur in the chain transfer agent that is present at the end of the polymer. The absence of any doublets between 5ppm and 6ppm also indicate that all monomer was removed. Some minor solvent impurities can be observed too.

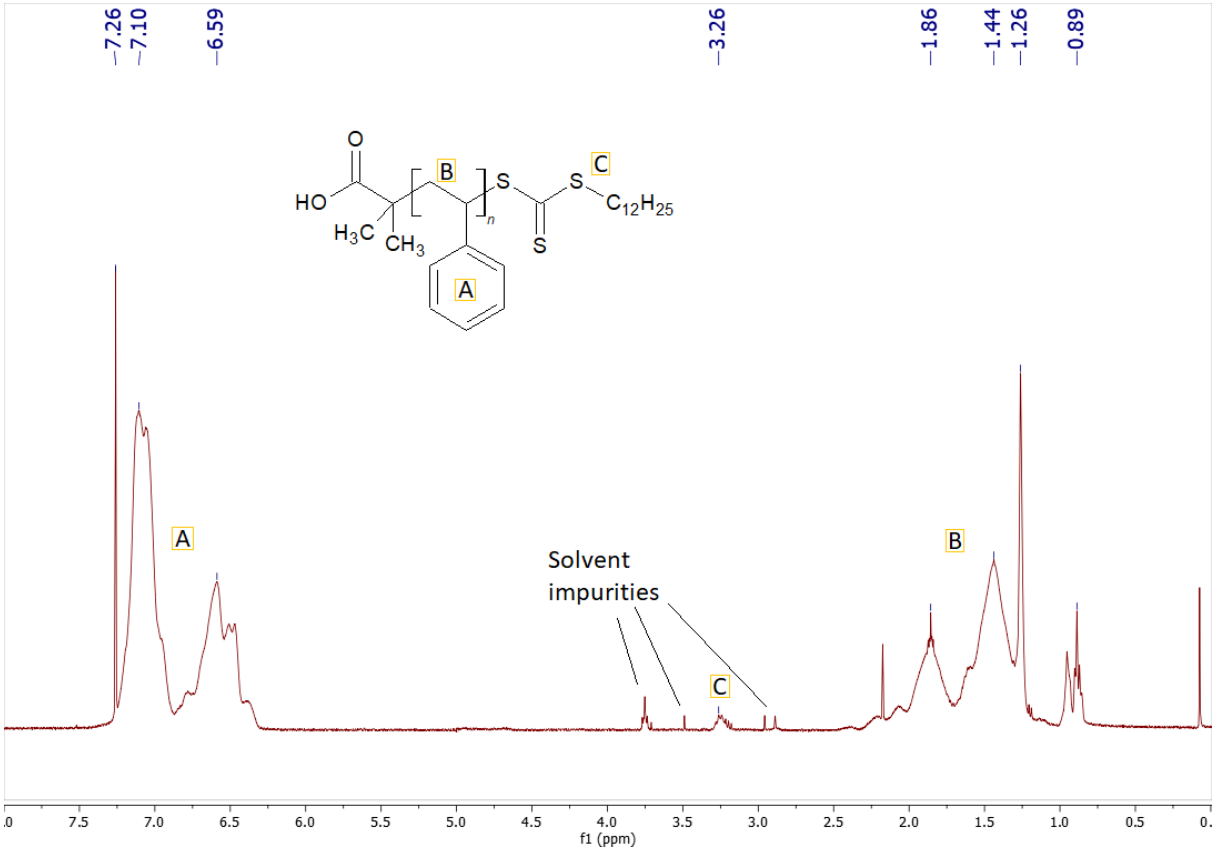

Figure 8 The monomer-free NMR spectrum of RAFT polymerisation polystyrene (PS_{30}) in $CDCl_3$.

4.2 RAFT synthesis of PS-*b*-PtBA

4.2.1 PS-*b*-PtBA exploration

Once the master batch of PS was obtained, the second block was ready to be attached. This involved the addition of tert-butyl acrylate (tBA) monomer to form the second block of the diblock copolymer. The target for the conversion of this reaction was set to 50% and was expected to take 7 hours. The synthesis was performed using anisole as a solvent, because tBA does not dissolve its own polymer unlike styrene. The first experiment involved taking samples during the reaction to gain knowledge on the reaction speed and curve. These samples were measured using the NMR. The conversion was calculated by comparing the monomer peak area to the aromatic part of styrene. Since the aromatic styrene region will not change during the reaction, it can be considered the same as an internal

standard. By setting the aromatic region the same for each sample, the integrated peak area of the monomer at T0 can be compared to the integrated peak area of the reaction samples.

The resulting conversion curve is shown in Figure 9. The first data point gave an indication that some inhibitor might have been present after the filtration of the monomer. Once the first data point is excluded a very solid linear progression is observed. The conversion was faster when compared to the reaction speed of PS. The PtBA seems to react more easily, leading to a shorter reaction time of only five and a half hours to reach 50% conversion. This can be explained by taking the resonance structures of PS into account, which allow the radical to be delocalised due to the benzene ring. Because the PS radical is more stable due to resonance-delocalised radicals, the reaction speed is also slower. In the case of PtBA, while the acrylate can still offer a singular resonance structure using the double bonded oxygen, there are much less variations. As a consequence, this radical is less stable compared to a PS radical leading to a faster reaction time.

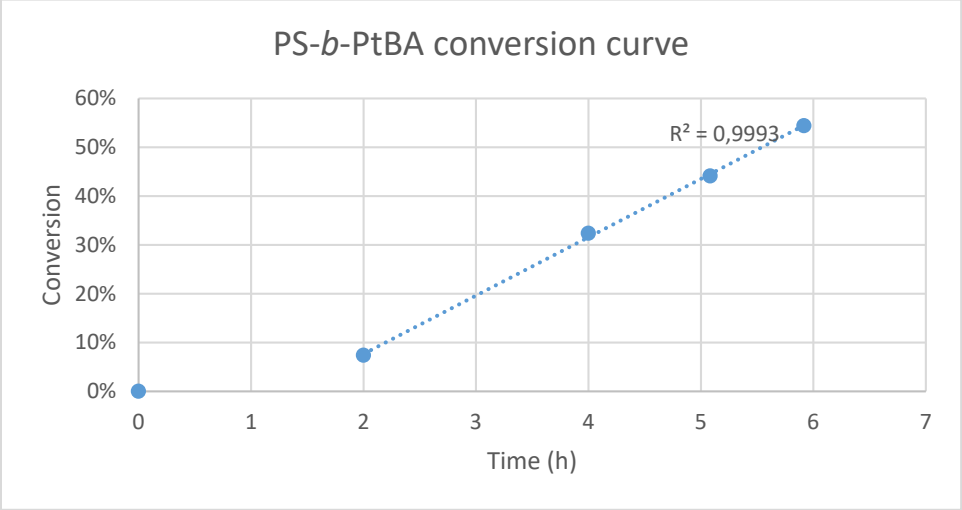

Figure 9 The conversion curve of the formation of the second block (PtBA)

The samples were also measured on the GPC to illustrate the progression of the reaction. Figure 10 shows the several samples that were taken at different times during the same PS-*b*-PtBA synthesis. Therefore, it shows the growth of the polymer chain length. The dispersity is also noted in the legend as PDI (poly dispersity index), which is also lowering as time progressed. This indicates that the polymerisation is a well-controlled process that gives a narrow distribution in chain lengths. The peak symmetry is important too, which indicates that chain length distribution is very similar. If the peak would be asymmetrical with the right side of the peak stretched out over longer, it would indicate many smaller chains. However, this not the case and a narrow chain length distribution is observed.

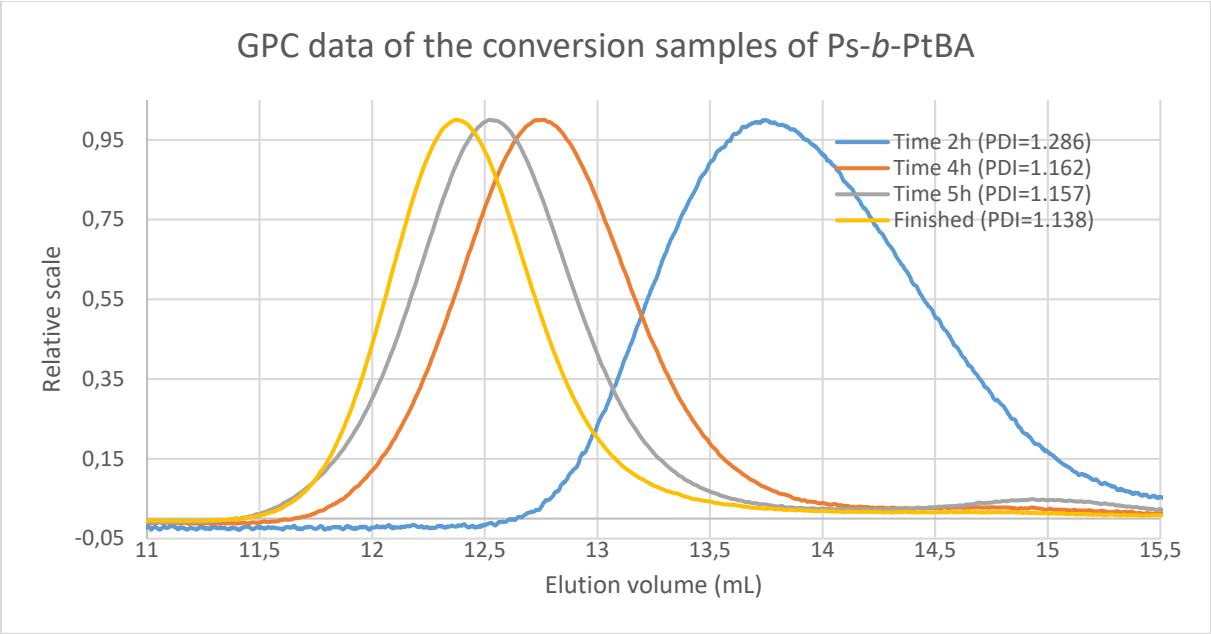

Figure 10 The GPC data of several samples taken from the same reaction mixture at different times with the finished polymer being PS_{30}-b-$PtBA_{330}$.

4.2.2 PS-*b*-PtBA synthesis

The final reaction scheme and conditions are depicted in Scheme 5. To obtain the dried polymer, the solvent has to be removed. This can either be done *via* dialysis or evaporation. The downside of dialysis is the long time it takes for all the anisole to be removed and the high boiling point of anisole prevent evaporation being an easy option. By switching the solvent from anisole to dioxane, the boiling point is lowered to a more easily removable temperature. This change in solvent showed no impact on the polymer reaction speed.

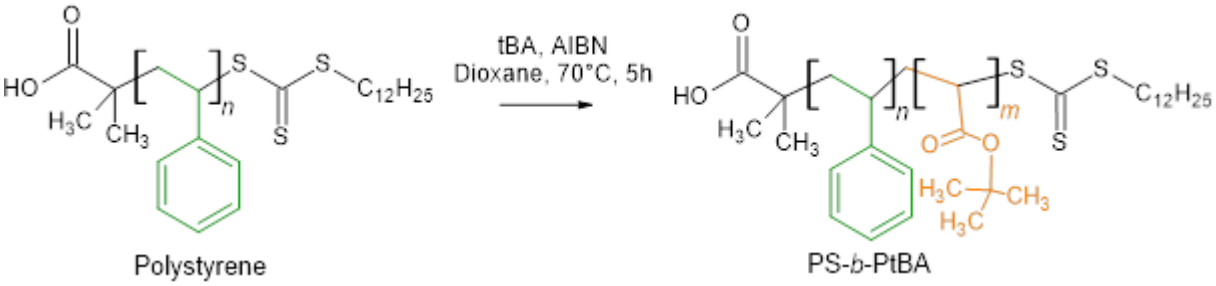

Scheme 5 The reaction scheme of PS-b-PtBA.

The tBA monomer present still needed to be removed from the obtained dry polymer. This was done by dissolving the material in THF and precipitating it in a 50/50 methanol/water mixture. This proved not to be the optimal precipitation method as the resulting yield was low. The method was chosen because both PS and PtBA mono-polymers do not dissolve in water. The supporting information of Xu et al.[34] showed the use of a 50/50 methanol/water mixture to precipitate PtBA, however this was cooled. The mixture was copied as 90% of the PS-*b*-PtBA diblock copolymer is PtBA. Since polystyrene also does not dissolve in methanol or water, this seemed to be a good mixture. Due to the low yield (25%-28%) from this mixture, subsequent syntheses used a different precipitation.

As it turns out, the PS-*b*-PtBA diblock copolymer actually dissolves in methanol itself. This makes the precipitation step somewhat easier, as the methanol can now be poured directly into demineralised water. However, this led to an issue at the surface of the water. The polymer precipitated quickly but

also stayed at the top of the water. This led to clumping of the polymer and meant that there was very poor contact between the methanol and the water. By using a glass pipet and slowly injecting directly into the middle of the solution while stirring, the contact between the droplets and the water was greatly increased, leading to a more efficient precipitation. This resulted in a decent yield (50%-57%) with a cleaner polymer, although there was still cloudiness present in the mixture, indicating still dissolved polymer (albeit only a tiny amount).

To further increase yield, the dissolved polymer can be extracted too. This was done using vacuum filtration and pouring the mixture on a filter. This method helped to extract more polymer from the mixture and increased yield. However, the yield increase (~10%) was not substantial enough to perform the vacuum filtration every time. An overview of yields is given later on in section 4.5.

4.2.3 PS-*b*-PtBA NMR analysis

Figure 11 shows the NMR spectrum of PS-*b*-PtBA in $CDCl_3$ (7.26ppm). There are some similarities when comparing this NMR spectrum to the NMR spectrum of PS in section 4.1.3. The first is the aromatic region between 6.3ppm and 7.5ppm containing the signal from the styrene ring, which again is labelled A. The other similarity is the aliphatic region between 0.8ppm to 2.5ppm and contains the backbone of the diblock copolymer. The introduction of a PtBA block that is close to 10 times as long as the PS block, means a weaker signal for the aromatic region A. The introduction of 9 very similar hydrogens found in the tert-butyl moiety leads to a dominant peak at 1.4ppm. The E peak is so large that the previously visible CTA peak is lost in the noise. The purity of the sample is good and can be seen by the absence of doublet monomer peaks between 5.5ppm and 6.5ppm.

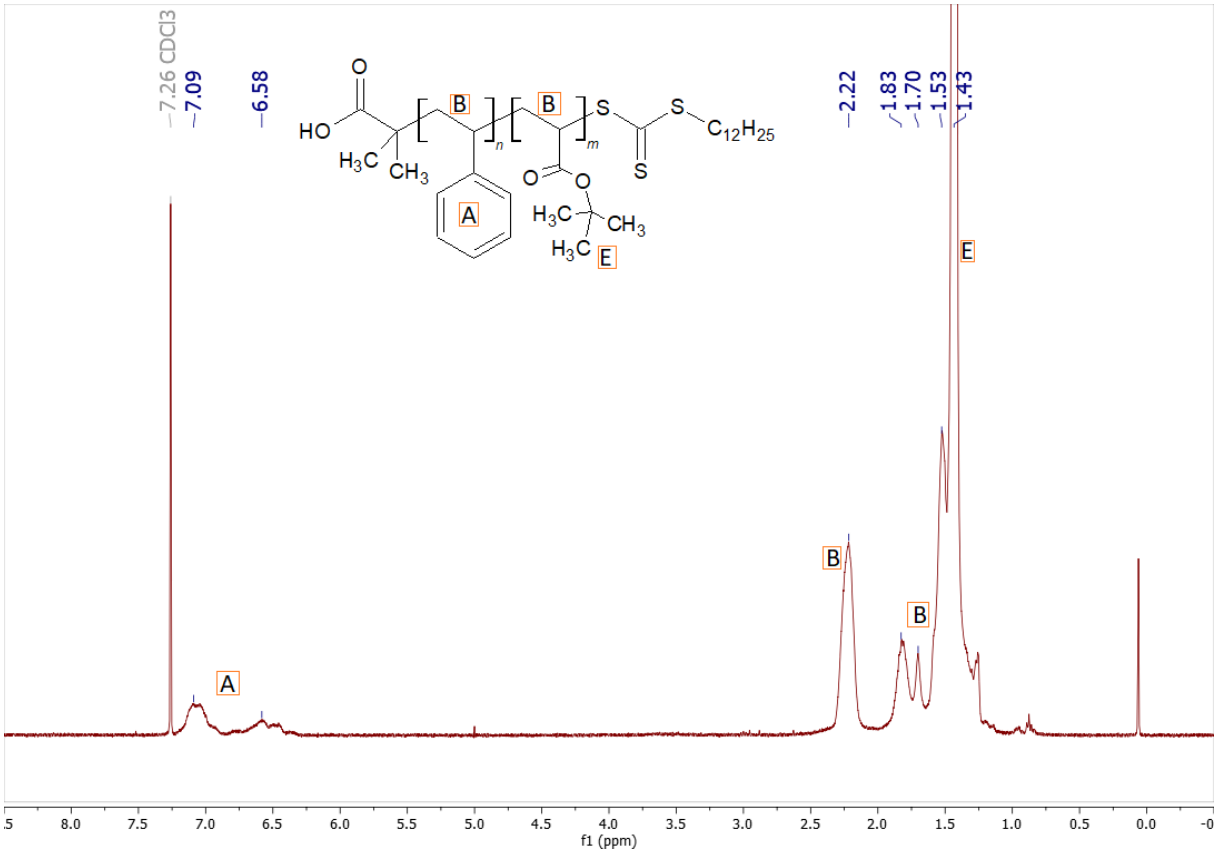

Figure 11 The NMR spectrum of PS_{30}-b-$PtBA_{330}$ in $CDCl_3$. The introduction of the PtBA block leads to a large peak at 1.4ppm.

4.3 Deprotection synthesis of PS-*b*-PtBA to PS-*b*-PAA

4.3.1 Ester hydrolysis synthesis route options

After the PS-*b*-PtBA diblock copolymer was obtained, it needed to be converted into PS-*b*-PAA. The most commonly used method involves an ester hydrolysis using trifluoroacetic acid (TFA) and dichloromethane (DCM). The acid starts the hydrolysis and leads to the formation of tert-butyl alcohol and poly(acrylic acid). This ester hydrolysis has a long reaction time of 72h and does not fully convert every PtBA segment into PAA, leaving it below 100% removal according to Filippov et al.[33].

In this article[33], another synthesis route option was offered to increase the removal efficiency. This was done using HCl as the acid and dissolving the polymer in 1,1,1,3,3,3-hexafluoro-2-propanol (HFIP). This led to an increase in deprotection efficiency and a faster reaction time, minimising it to four hours. They argued that there are two factors that improve the efficiency when using HCl/HFIP instead of TFA/DCM. The first is that DCM is a non-solvent for PAA, which prevents contact between partially deprotected intermediate polymer and the acidic medium. The second reason is the formation of dimers formed by the carboxylates, which happens in apolar environments. Note that this dimer formation occurs between TFA and the newly formed PAA. This leads to a further decrease in contact between the acidic medium and the polymer. In comparison to HCl/HFIP, these factors are not an issue. The HFIP does not precipitate the product, leaving it in contact with the acidic medium. The HCl is a non-carboxylic acid and cannot form dimers with the product, preventing contact loss.

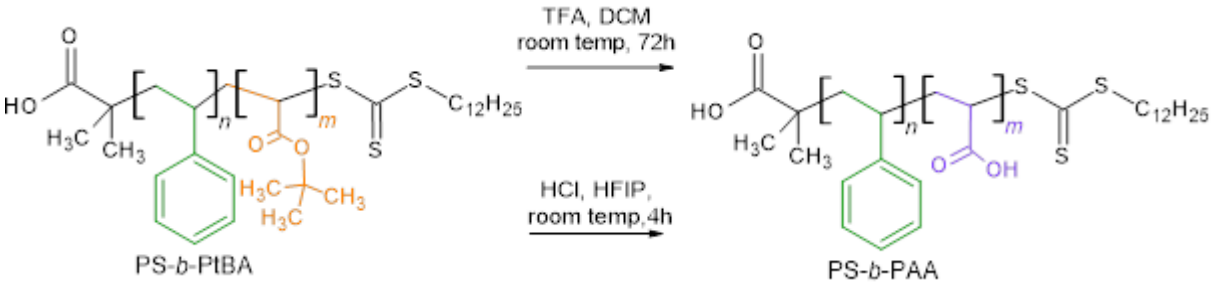

Scheme 6 The two different reaction scheme routes to change PS-b-PtBA into PS-b-PAA. The HCl/HFIP route was used throughout the research due to better results.

Scheme 6 depicts the two different options for deprotection routes. All the advantages in reaction time and deprotection efficiency that the HCl/HFIP route offered made this pathway more promising than the other. Throughout the rest of the research, the HCl/HFIP method was used.

After the reaction, the polymer was dissolved in THF and precipitated in n-pentane to remove impurities from the diblock copolymer. After overnight drying under vacuum at 40°C the dry polymer was obtained for NMR analysis. No GPC analysis was performed using this polymer, as the polar acrylic acid would not pass through the column. The yields of this step stayed consistent (83%-87%).

4.3.2 PS-*b*-PAA NMR analysis

Figure 12 shows the NMR spectrum of PS_{30}-*b*-PAA_{330} in deuterated DSMO. The measured range was widened to between 14pmm and -2ppm. The widened measuring range was done to see the new acid peak that was formed round 12 ppm. The same regions can be seen as in the NMR spectra of previous steps. The aromatic region A is seen at 6.3ppm to 7.5ppm and originates from the styrene ring. The aliphatic region B can be seen between 0.8ppm to 2.5ppm and contains the backbone of the diblock copolymer. During future experiments, this F peak was usually more pronounced and sharper. However, this specific sample contained water (as is seen at 3.33ppm) and this led to the exchange of hydrogen/deuterium between the PAA and the water, resulting in a broadened and diminished signal.

An NMR spectrum with a more typical acid peak can be seen in appendix 7.1.4. The purity of the sample is lower because of a tiny peak at 1.2ppm which indicates a small amount of tert-butanol is still present, in addition to the water contamination. The amount is negligible and can be removed with extra precipitation steps if necessary.

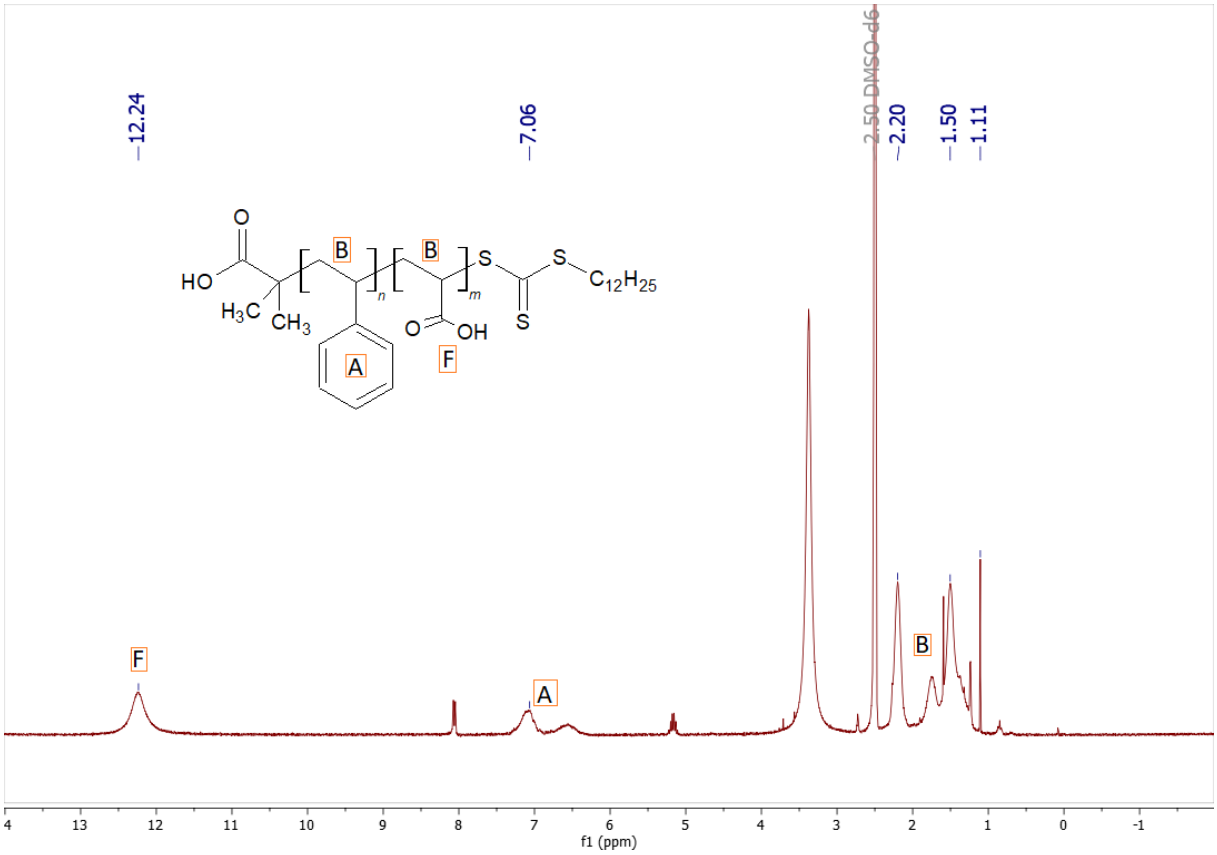

Figure 12 The NMR spectrum of PS_{30}-b-PAA_{330} in deuterated DMSO.

4.4 Chain transfer agent removal

4.4.1 Chain transfer agent removal options

During the research, it was suspected that CTA was changing the AB diblock copolymer character into an ABA diblock copolymer character, as explained in section 2.7. This meant that the PS-*b*-PAA diblock copolymer needed to be made without the CTA. There were two approaches to this problem. The first is changing the CTA itself. The issue is the long C_{12} chain that is present in DDMAT, as this is hydrophobic and could present itself as an extra block. By changing DDMAT to a different CTA with a shorter/different end group, it would be possible to prevent this triblock character issue. This would change all the reactions that were performed and reported in this thesis, while the effects of the CTA were still uncertain.

The other solution to this problem is removing the CTA once it is no longer needed. If the CTA has performed the intended task, it can be removed using the method by Discekici[32] as described in section 2.7. The main benefit of using this photocatalytic chain transfer agent removal reaction is the absence of chain doubling termination reactions.

4.4.2 Chain transfer agent removal of PS-*b*-PtBA-CTA

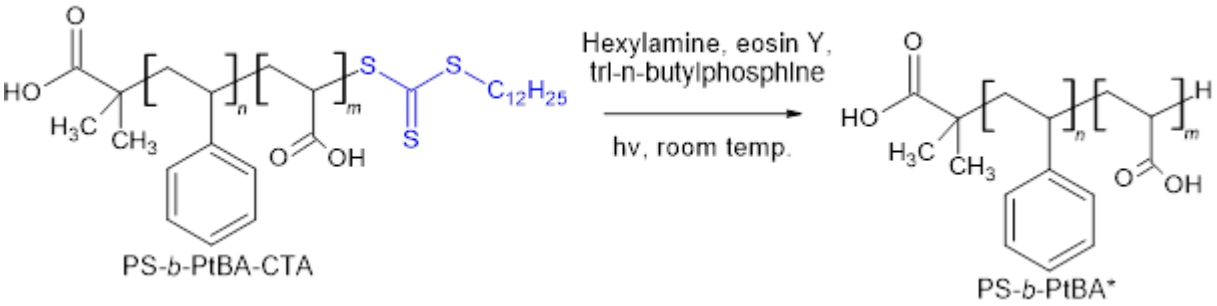

Scheme 7 The reaction scheme showing the photocatalytic removal of the chain transfer agent of a RAFT polymerised PS-b-PtBA diblock copolymer. The star in PS-b-PtBA indicates the absence of a CTA.*

Scheme 7 shows the reaction scheme of the CTA removal. It is the photocatalytic removal of the tri-thio moiety from the PS-*b*-PtBA diblock copolymer. It starts with the substitution reaction between the amine and the tri-thio moiety. This leaves the polymer end capped with a thiol group as shown in Scheme 2. The photocatalyst will then activate the sulphur of the thiol, which leads to the departure of a proton, leaving a radical on the sulphur. The radical on the sulphur is then quickly reacted with the phosphine, transferring it to the polymer. The radical on the polymer then abstracts the hydrogen from another thiol polymer, repeating the cycle.

It is important to note that the removal of the CTA could also be stopped earlier. If only the substitution reaction is performed, then the polymer would be end capped with a thiol. One might suggest to end the CTA removal here. The functionality of a single thiol group should not impact the AB diblock character of a single diblock copolymer and change it into a ABA triblock character. Moreover, one could say it might even be beneficial to the interfacial properties as a polar group would extend into the solution and promote the zipper brush shape. However, there is an issue with this approach and mainly lies with the reactivity of the thiol group. A thiol group can react in various manners and lead to unintended side reactions. An example is the formation of a disulphide bond from two thiols. If a thiol end capped diblock copolymer finds another one, the end capped thiol groups can oxidise into a disulphide bond. This is very similar to the concept of chain doubling termination reactions which attaches both ends of the polymer to each other. This would result in a full PS-PAA-S-S-PAA-PS multi-block copolymer, which would likely be unfavourable for the performance of the antifouling coating.

The CTA removal synthesis was performed on two different polymers. The first polymer was the PS-CTA intermediate homopolymer and was used to test the viability of the synthesis. The strong yellow colour that is present in the material due to the DDMAT is a good indication to see if the CTA removal was performed correctly. The second was the PS-*b*-PtBA diblock copolymer which was the intermediate polymer before the deprotection step. This intermediate PS-*b*-PtBA diblock copolymer was chosen instead of PS-*b*-PAA because both blocks have similar properties like hydrophobicity and easily dissolve in the same solvent. In addition to the properties of the PS-*b*-PtBA polymer, it can also be measured on the GPC to detect any peak doubling. This is not possible for the PS-*b*-PAA due to the polarity of the monomeric units.

4.4.3 CTA removal

The removal was performed as described in section 3.6. A picture illustrating the setup that was used can be seen in Figure 13 and Figure 14. The LED lights were placed on the inside of a cardboard ring and set to emit a blue light. The blue light was used to activate the photocatalyst eosin Y in the mixture. The reaction was left overnight under inert atmosphere and after about 16 hours of reaction time it was noted that solvent had evaporated and escaped out of the flask. After the addition of extra solvent, it was left to complete the reaction. A small amount of white power was obtained after all the precipitation steps were taken.

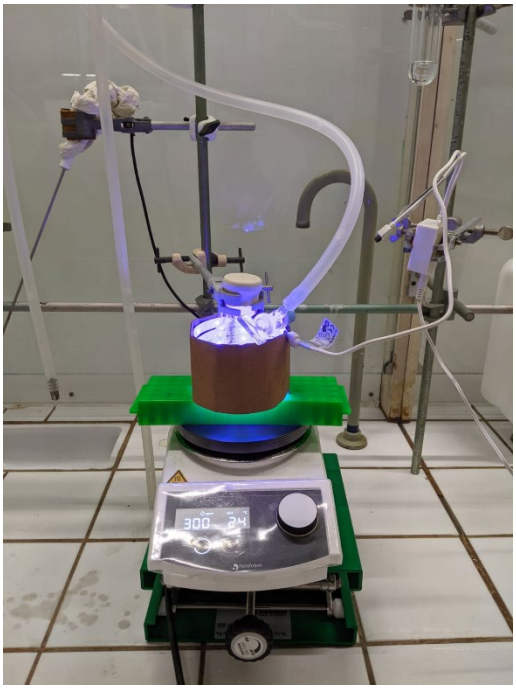

Figure 14 An overview photograph of the reaction setup for the photocatalytic removal of the CTA.

Figure 13 A close up photograph of the reaction setup for the photocatalytic removal of the CTA.

The difference in colour between the two PS polymers with and without CTA is clearly visible in Figure 15. The intense yellow colour that is visible on the left is the DDMAT that is still attached to the polymer. On the right of the picture is the CTA free polymer which shows to be white. Because the only yellow colour that is introduced in the polymer is the DDMAT, it can be seen that it is removed. To further support this statement, analysis with NMR, GPC, and UV/VIS was performed.

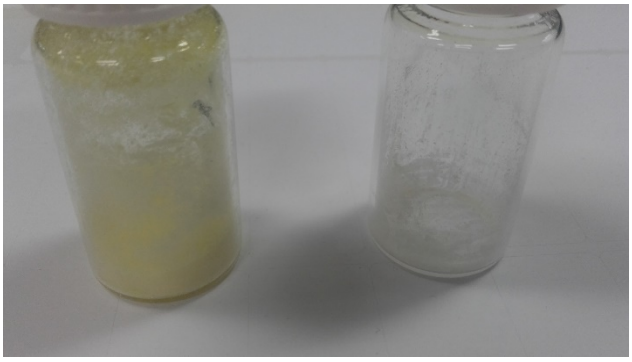

Figure 15 The two different polystyrene polymers. On the left is the regular PS with CTA and on the right the new PS without CTA.

4.4.4 PS CTA removal analysis techniques

4.4.4.1 NMR

The first analysis techniques that was used to check if the CTA was still present was NMR. The NMR of conventional PS with CTA was shown in Figure 8 in section 4.1.3 and it demonstrated that there was a small but visible peak at 3.25 ppm. This peak is correlated to the hydrogen next to the sulphur that is present in the DDMAT. A new NMR was taken from the white dried supposedly CTA free PS_{30} homopolymer and is shown in appendix 7.1.3. This was placed over the previous NMR that was taken of the PS_{30} with CTA present and is shown in Figure 16.

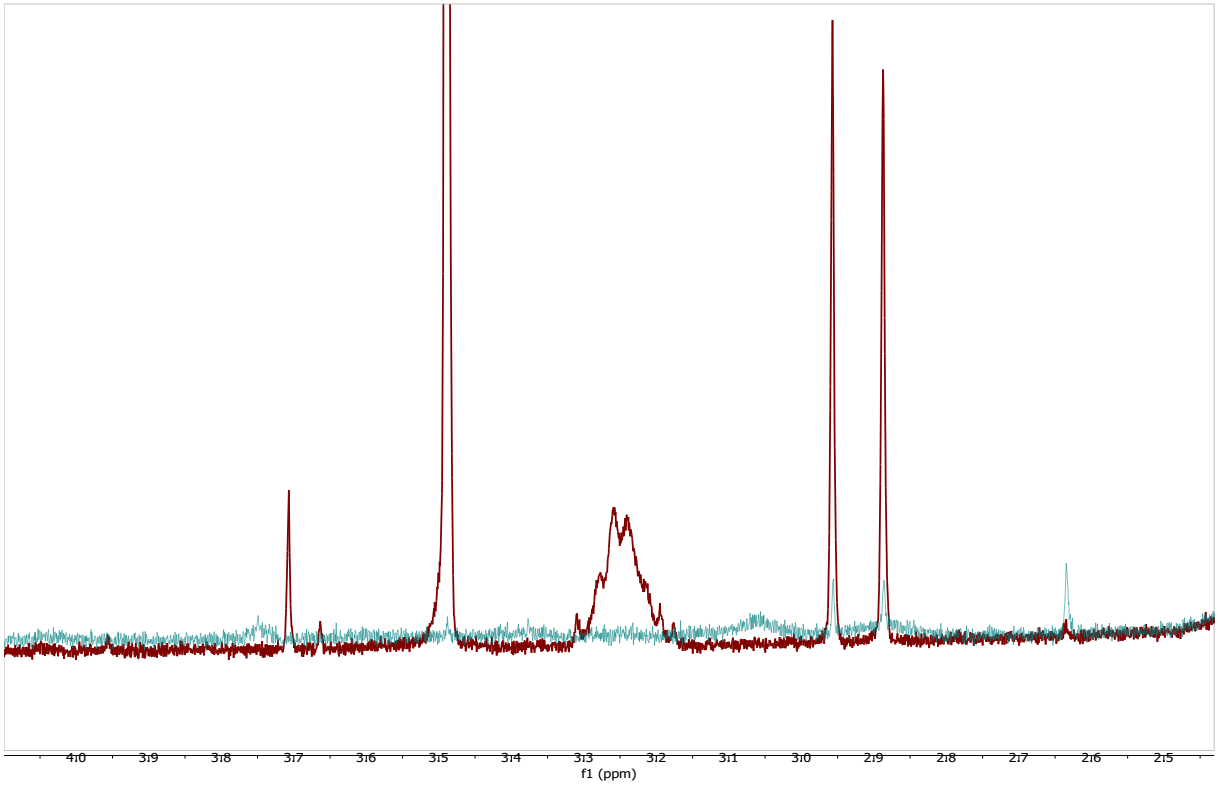

Figure 16 An overlay of the NMR spectra of both the CTA and the CTA free PS polymers. The red line is PS with CTA and the blue line is PS without CTA. The peak at 3.25 is no longer present, indicating the removal of the CTA.

Figure 16 shows the difference between the polymer around 3.3 ppm. The peak at 3.25 ppm is clearly visible for the red line, but not for the blue line. This indicates that the removal of the CTA has progressed to completion. An article by Zhang et al.[35] reported an NMR of HS-PS-COOH that showed that the thiol group would still be visible if connected. Because the blue line shows no peak in this area whatsoever, it is safe to state that the entirety of the tri-thio moiety was fully removed from the PS.

4.4.4.2 GPC

Both the CTA and CTA free PS polymers were measured using GPC. The GPC data obtained from these measurements were plotted in the same graph, which can be seen in Figure 17. It depicts two lines that show a negligible difference between the two measured polymers. This is intended and confirmed by the research this synthesis was based on[32]. There is no difference in dispersity between the two. The CTA free PS does not exhibit any peaks that would indicate chain doubling effects. The similarity between the two samples is correct and expected. Concluding that the CTA removal was successful.

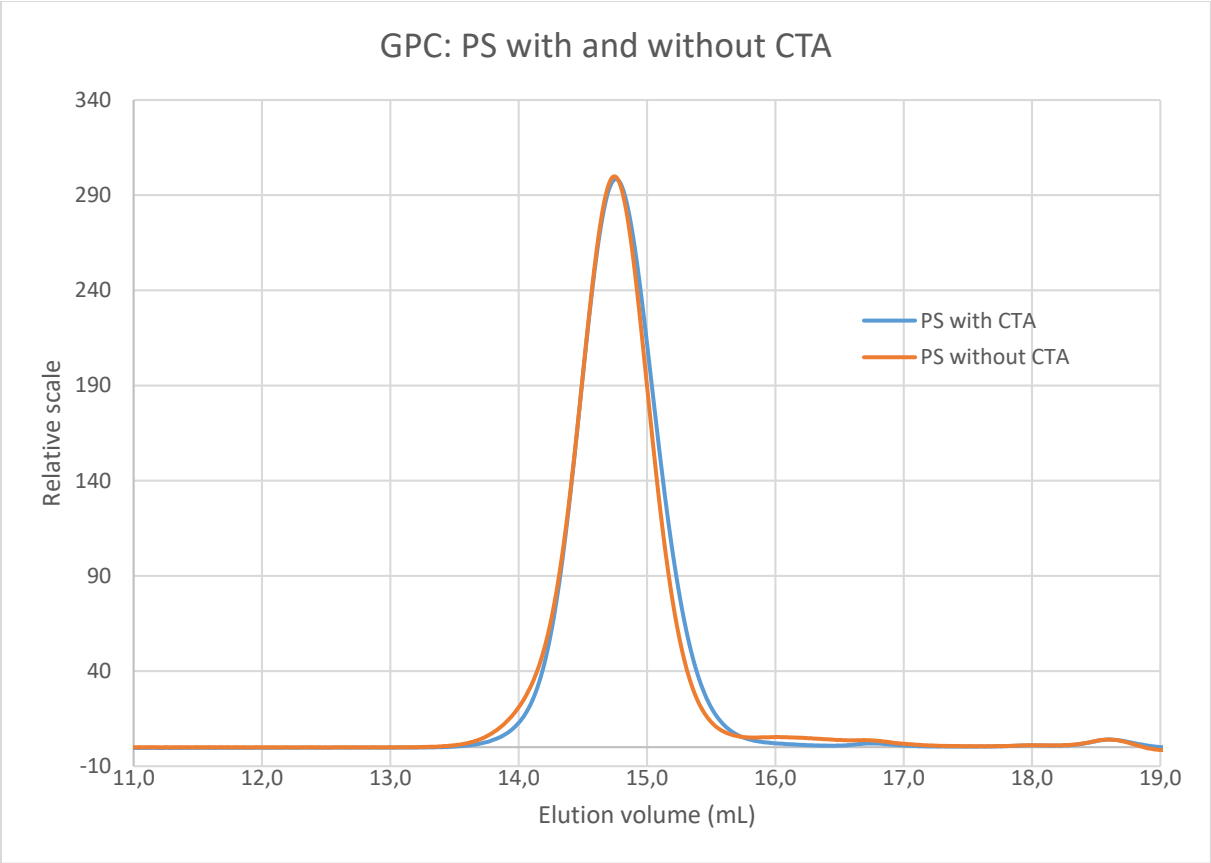

Figure 17 The GPC data showing the same PS with CTA and without CTA. There is no significant difference between the two different polymers.

4.4.4.3 UV/VIS

The PS with and without CTA was also analysed using UV/VIS to double check if any CTA was still present. The polymers were analysed using a quartz cuvet because the plastic variant would be dissolved by the solvent. The data is depicted in the graph that is shown in Figure 18.

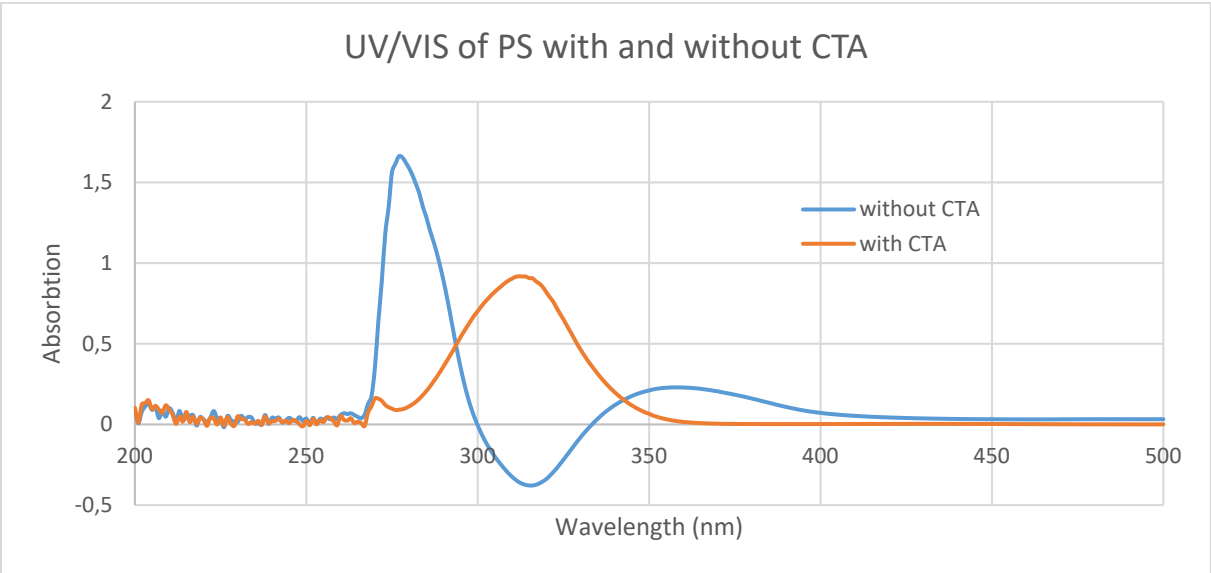

Figure 18 The graph shows two curves of UV/VIS data of PS with CTA and PS without CTA. The yellow CTA absorbs around 310nm and is visible in the polymer with CTA present. The PS without CTA shows an absorbance at 279nm but not around 310nm, indicating CTA removal.

The orange curve shows the normal PS with CTA. A yellow material would absorb blue light to be seen by humans as yellow. There is a noticeable absorbance around 310nm which indicates that the CTA is attached to the polymer. This would explain the yellow colour that is observed by eye as shown in Figure 15.

The blue curve shows the new PS without CTA. The white polymer has an absorbance around 279nm and a negative absorbance at 310nm. Eosin Y is the photocatalyst that was used during the synthesis but if this was still present, the material would be red and show absorbance at 500nm. The important factor is the negative absorbance at 310nm which means that no CTA was present in the polymer.

4.4.4.4 Summary

All analysis techniques indicated a successful removal of the CTA from the PS_{30}. This meant that the experiment could be repeated on the PS-*b*-PtBA diblock copolymer to obtain PS-*b*-PAA without CTA.

4.4.5 PS-*b*-PtBA CTA removal

The CTA removal synthesis was performed using the PS_{30}-*b*-$PtBA_{370}$ diblock copolymer. The synthesis was performed with a similar setup as described and depicted in 4.4.3. This time there was no leakage or evaporation of solvent compared to the PS CTA removal synthesis. The initial polymer had a very slight yellow hue but any difference was too difficult to capture on a photo. After the experiment was finished, a dry polymer with a light red hue was obtained. This indicated that there was still photocatalyst present in the polymer and led to a repetition of the precipitation steps. Afterwards a dry polymer with a very slight red hue was obtained and was used in subsequent steps.

Usually the NMR is shown first, however for the PS-*b*-PtBA diblock copolymer it is unusable. The tBA adds a very large peak at 1.4 ppm that towers over the others. This means that the peak at 3.25 from the DDMAT is so small that it is no longer distinguishable from the noise. This means that the NMR cannot show an accurate difference between the two polymers with and without CTA and is therefore excluded from this report.

4.4.5.1 GPC

The PS-*b*-PtBA polymer with and without CTA were both analysed using GPC. The data is shown in Figure 19. It shows that the difference between the two polymers is negligible. The orange line that depicts the CTA free version does not exhibit any peak doubling that would indicate unwanted termination reactions. Both curves have a similar dispersity and a comparable Mn. This was in line with previously found GPC results and expected to occur.

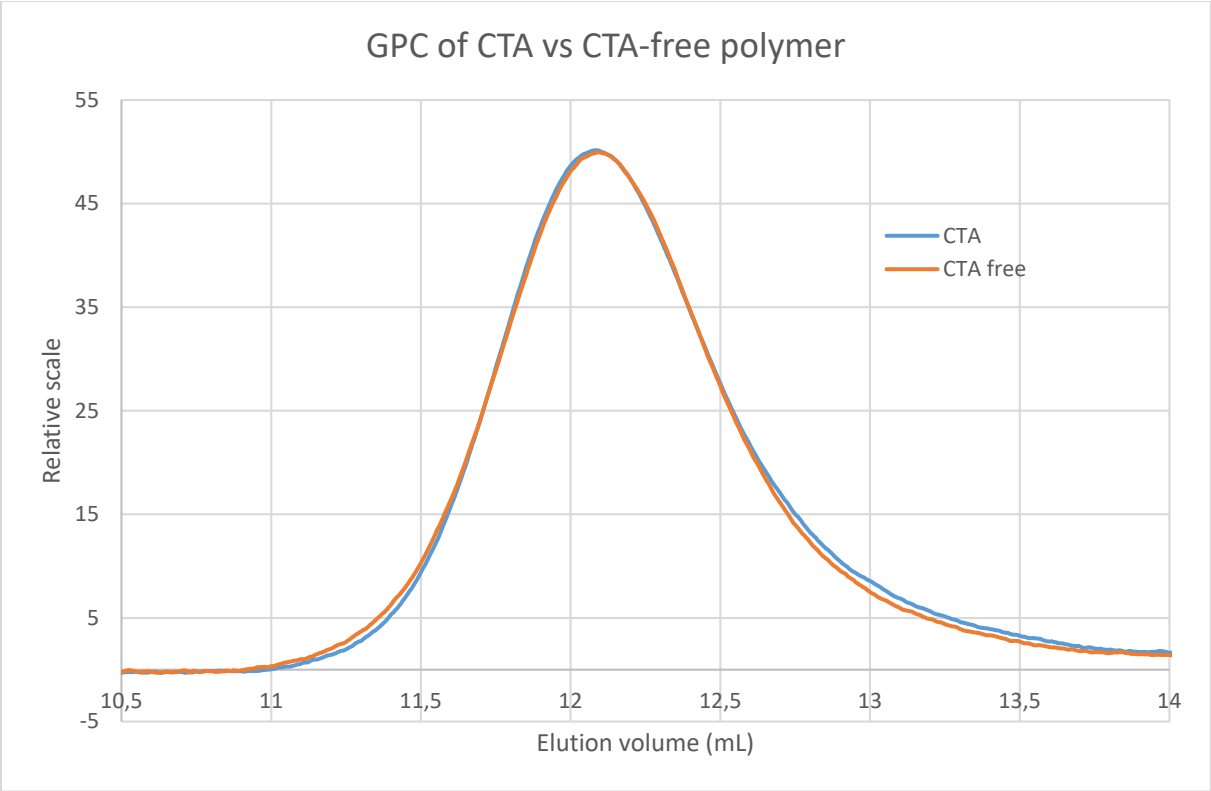

Figure 19 The GPC data of CTA and CTA free versions of PS-b-PtBA. There is a negligible difference between the two curves, indicating that no termination reactions have taken place.

4.4.5.2 UV/VIS

In order to check if the polymer would still contain any DDMAT after the CTA removal synthesis, a UV/VIS experiment was performed. Figure 20 shows various curves of increasing concentration. No absorption is observed at 310nm indicating that no CTA is present in this polymer.

In order to double check if the CTA that was present in the normal PS-*b*-PtBA would be visible using UV/VIS, a small amount of this polymer dissolved and measured. Different concentrations were used until the absorption was clearly visible. This increase in absorption can be seen in Figure 21 and shows a clear increase in absorption at 310nm, indicating that CTA is present in the polymer. The very slight red hue that was observed in the polymer was not observed using UV/VIS and should be visible at 500nm if it were present. Because nothing was observed using UV/VIS and subsequent steps made the polymer white, it was not deemed to be an issue.

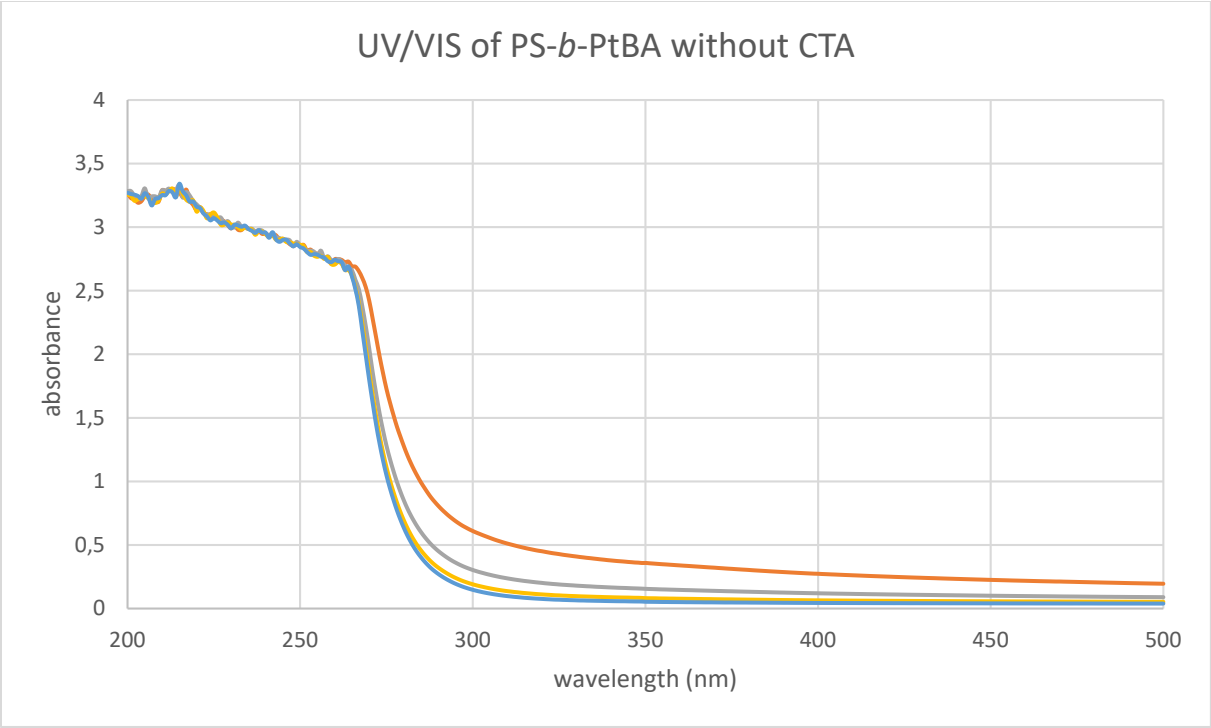

Figure 20 The PS-b-PtBA without CTA was measured at different concentrations and no peak was observed at 310nm.

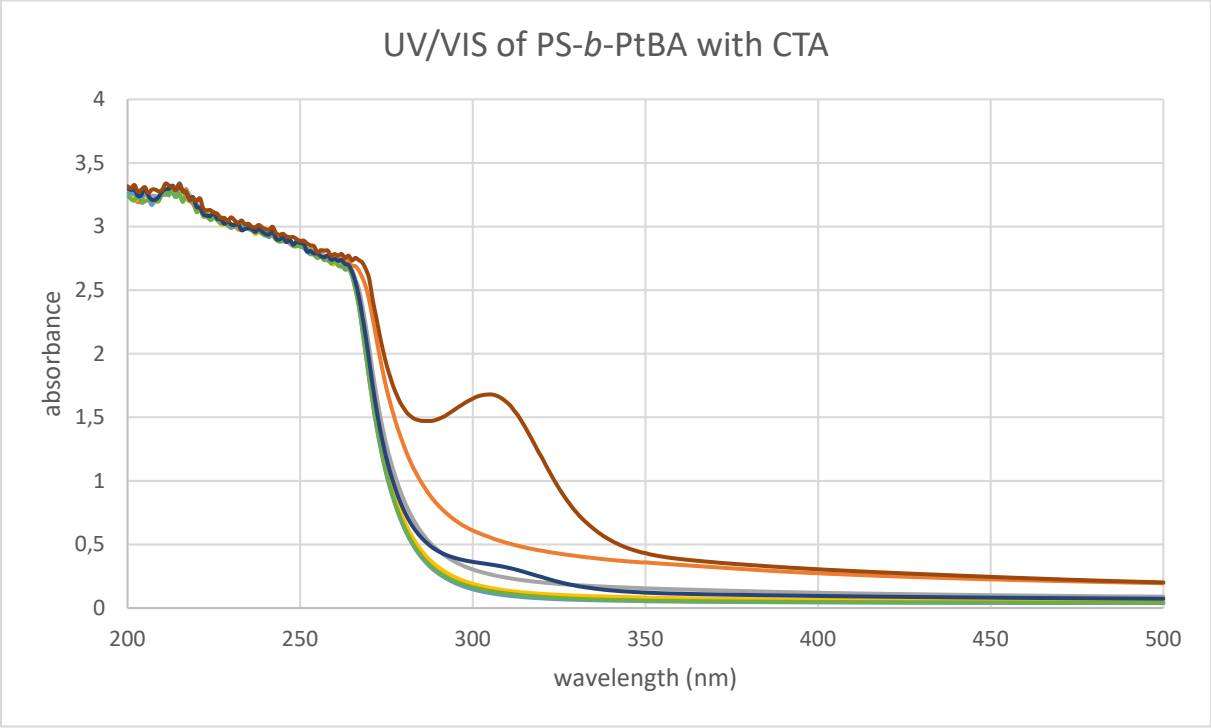

Figure 21 The addition of PS-b-PtBA with CTA led to an absorption at 310nm indicating that it is possible to measure this CTA on the UV/VIS.

4.4.5.3 Summary of PS-b-PtBA CTA removal

A clear indication of CTA removal was observed with every technique used. This meant that it was possible to continue and measure the effects CTA removal had on the polymer brush. The PS-*b*-PtBA needed to be converted to a PS-*b*-PAA diblock copolymer, which is the final product and is the polymer that can form micelles. The ester hydrolysis that is described in section 3.5 was used to deprotect the

PS-*b*-PtBA and form PS-*b*-PAA. After the precipitation and drying steps, this polymer was obtained as a dry white powder.

4.4.5.4 DLS

An important feature to measure would be any indication of the shape of the micelles that could be formed by the PS-*b*-PAA diblock copolymer in solution. To do this, the polymer was measured using dynamic light scattering (DLS). Specifically, DLS allows the particle size to be measured using the way light is scattered by the particles that are suspended in solution. If the polymer aggregates and forms a micelle, then there would be an obvious distinction between the sizes of the different possible micelles. A flowerlike micelle is typically bigger than the spherical micelle. Therefore, a smaller particle size could indicate a change in micelle structure from flowerlike to spherical.

Both the PS-*b*-PAA with and without CTA were measured using DLS with ethanol as solvent. The concentrations were set at 10mg/ml and each sample was filtered before the measurement to remove impurities. Each measurement was performed five times in a row to check for repeatability. The data of the results was exported as images and displayed as the DLS showed.

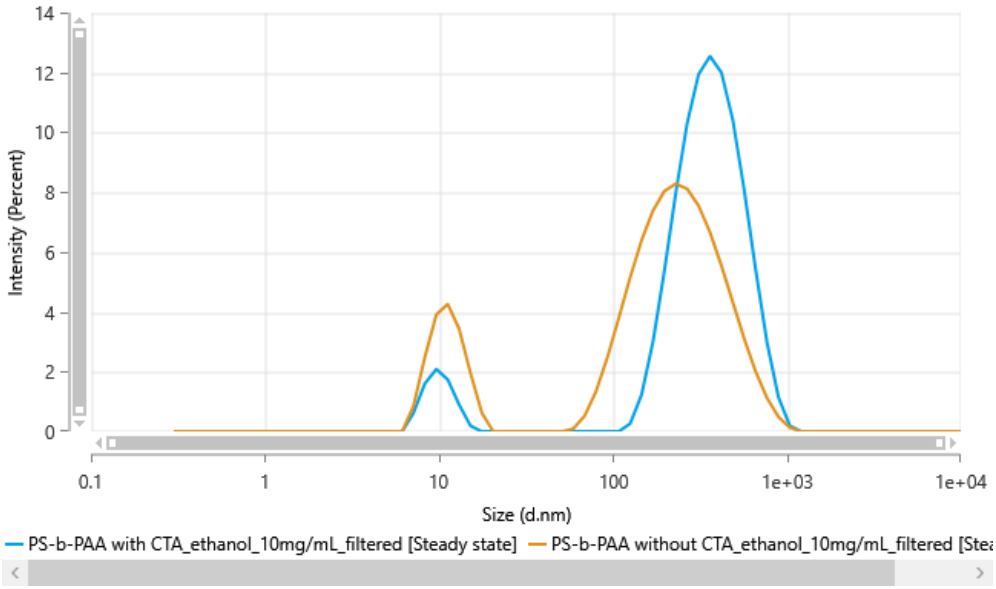

Figure 22 The DLS data of PS-b-PAA with and without CTA. The graph shows the difference in particle size and the number of particles with that size is tied to the intensity.

Figure 22 shows the particle sizes of both PS-*b*-PAA with and without CTA. The blue line shows that the PS-*b*-PAA with CTA is more likely to aggregate and form large particles. The intensity difference between the 10nm diameter particles and ~400nm diameter particles shows that a large portion of the available material is aggregated. The orange line shows that the PS-*b*-PAA without CTA is less likely to aggregate than the version with CTA. This can be seen by the shift towards a slightly lower particle size compared to the blue line. In addition to this, it is also much broader than the blue line, indicating a much higher particle size dispersity. Lastly, a more equalised ratio between the 10nm and ~200nm peaks is observed. The correlation curve can be found in appendix 7.1.4 and shows the improved correlation when CTA is removed.

A confident statement about the shape of the micelles cannot be made using these results. It seems that there is less large size aggregation if PS-*b*-PAA does not contain CTA. This can still be beneficial for the zipper brush polymer application. The PS-*b*-PAA with and without CTA were both handed over for evaluation of the zipper brush performance.

The finished polymers were analysed by Annemarie Maan using Quartz crystal microbalance with dissipation monitoring (QCM-D) and focused on the difference between properties in zipper brush functionality. It was concluded that the removal of CTA from PS-*b*-PAA does not lead to any significant difference in interfacial properties when the diblock copolymer is used during zipper brush formation. While a difference in micelle structure might have occurred, it had no effect on the anti-fouling performance using the current application method.

4.5 Overview of polymers

An overview of the most important synthesised polymers is shown in Table 2. It displays the different polymers that were synthesised along with the ratio of styrene compared to total polymer length in percentage. The yield column shows the various amounts of yield. The percentage number describes the yield for each formation step. If the polymer needed a deprotection step, then the deprotection yield is also shown below.

Table 2 The overview of the important synthesised polymers.
** = The removal of CTA instead of a block formation step.*

Name	Polymer	Ratio	Yield	Yield %	Yield Deprot. %
IR006	PS_{30}		07,22g	72%	
IR012	PS_{30}-b-PAA_{330}	9%	0,123g	28%	85%
IR014	PS_{30}-b-PAA_{540}	5%	0,120g	25%	83%
IR017	PS_{30}-b-PAA_{100}	23%	0,129g	50%	89%
IR018	PS_{30} (no CTA)		~20mg	33%*	
IR024	PS_{30}-b-PAA_{370}	7,5%	0,089g	57%	83%
IR025	PS_{30}-b-PAA_{370} (no CTA)	7,5%	0,372g	66%*	86%

The yield of the initial synthesis of PS is adequate and was slightly lower than expected due to extra washing steps. The precipitation usually goes more smooth than displayed by yield here. The yield of the PtBA addition step was very low at first, with only 25 and 28%. This was due to the difficult precipitation of the washing step with the methanol/water mixture. The method was altered to the version that included dissolving the polymer in methanol and adding it to water, and that led to a better precipitation. This step did include some losses due to the polymer sticking to the outside of the pipet, but the yield was brought up to around 50%.

The deprotection yields stayed very consistent over many experiments. The yield could be improved by extra washing of the pipets, but the extra time would likely not lead to a substantial enough increase in yield. The yields of the * CTA removal steps were decently enough as well. The low 33% yield was due to the low amount of initial material, combined with the difficult precipitation step. The washing step showed a cloudy waste, indicating that some polymer was still dissolved. The 66% yield was an improvement and was the result of improved precipitation methods.

5 Conclusion

This thesis reports the synthesis of a polystyrene-*b*-poly(acrylic acid) diblock copolymer via RAFT polymerisation. A method to reliably perform the syntheses of PS, PS-*b*-PtBA, and PS-*b*-PAA were reported and allows flexibility in chain lengths and block ratios. Several polymers with various ratios (1:4.3, 1:9, 1:18) and various length (PS_{30}, PAA_{100}, PAA_{300}, PAA_{540}) were produced. The deprotection step involving an ester hydrolysis was performed using a recently reported method involving HCl + HFIP and is considered a better and faster improvement over known conventional methods. The synthesised polymers were delivered and used in zipper brush experiments. The evaluation of the synthesised PS-*b*-PAA diblock copolymer regarding the performance during zipper brush polymer formation is not reported in this report and will be reported in a follow up study.

The thesis also reports the successful photocatalytic removal of the chain transfer agent from RAFT polymerised PS-*b*-PAA diblock copolymer. The hypothesis stating that the chain transfer agent was giving the PS-*b*-PAA diblock copolymer a triblock character that leads to flowerlike micelles was not proven or disproven. However, it can be stated that there was a change in particle size and number distribution when the CTA was removed. The removal of the CTA from the PS-*b*-PAA diblock copolymer made no difference for the zipper brush antifouling performance with the current application methods.

5.1 Outlook

The proposed synthesis method will result in an efficient and reliable way to make a PS-*b*-PAA diblock copolymer with a desired length and block ratio. Several options to improve the method are listed as follows:

- It is possible to use different CTAs and optimise the process for better reaction times or yields. However, the research into antifouling zipper brush polymer coatings is currently still in the exploratory phase. Optimisation might need to wait until the coatings is proven to work efficiently enough for use.
- While the CTA removal functions as expected, it might not be the most effective method to remove the CTA. In the research paper by Carmean et al.[29], the tri-thio moiety of the CTA was fully removed using N-ethylpiperidine hypophosphite (EPHP) and UV light. This prevents the need for a reactant that has to be handled in an inert environment. Another advantage is that there are no other reactants required. This experiment method was considered during this research, but the EPHP was unobtainable within the time frame.
- When the antifouling zipper brush polymer coating functions as intended and is efficient enough for larger scale production, then RAFT polymerisation might not be a cost effective synthesis method. A more efficient route that is less wasteful and has higher yields is preferable. An exploratory research into the various options of producing the diblock copolymer on a larger scale can be recommended.

5.2 Acknowledgements

I would like to sincerely thank Professor Marleen Kamperman for the opportunity to do my master research project in her group and for her supervision. Furthermore, I would like to thank my supervisor Annemarie Maan for her supervision help during my research. Her honest feedback not only elevated the quality of my research, but contributed to an interesting and enjoyable time. Her radiant personality and structured work made it so I couldn't wish for a better supervisor. Additionally, I would like to extend my gratitude to Theo Pelras for his help with the GPC measurements and Professor Wiebe de Vos for his guidance during the project. Last but not least, I would like to thank all the group members for making me feel appreciated and for providing a pleasant atmosphere.

6 References

(1) Maan, A. M. C.; Hofman, A. H.; de Vos, W. M.; Kamperman, M. Recent Developments and Practical Feasibility of Polymer-Based Antifouling Coatings. *Adv. Funct. Mater.* **2020**, *30* (32). https://doi.org/10.1002/adfm.202000936.

(2) Bixler, G. D.; Bhushan, B. Bioinspired Rice Leaf and Butterfly Wing Surface Structures Combining Shark Skin and Lotus Effects. *Soft Matter* **2012**, *8* (44), 11271–11284. https://doi.org/10.1039/c2sm26655e.

(3) Yang, W. J.; Neoh, K. G.; Kang, E. T.; Teo, S. L. M.; Rittschof, D. Polymer Brush Coatings for Combating Marine Biofouling. *Prog. Polym. Sci.* **2014**, *39* (5), 1017–1042. https://doi.org/10.1016/j.progpolymsci.2014.02.002.

(4) Occurrence, E.; Of, C.; Biocides, A. Biocides in Antifouling Paints : Environmental Concentration Levels and Distribution. **2014**, No. October, 52–56. https://doi.org/10.12910/EAI2014-45.

(5) Dafforn, K. A.; Lewis, J. A.; Johnston, E. L. Antifouling Strategies: History and Regulation, Ecological Impacts and Mitigation. *Mar. Pollut. Bull.* **2011**, *62* (3), 453–465. https://doi.org/10.1016/j.marpolbul.2011.01.012.

(6) Wiebe M. de Vos, Geert Meijer, Arie de Keizer, M. A. C. S. and J. M. K. Ultradense Polymer Brushes by Adsorption. *Soft Matter* **2009**, *6*, 2499–2507.

(7) Chen, W. L.; Cordero, R.; Tran, H.; Ober, C. K. 50th Anniversary Perspective: Polymer Brushes: Novel Surfaces for Future Materials. *Macromolecules* **2017**, *50* (11), 4089–4113. https://doi.org/10.1021/acs.macromol.7b00450.

(8) Kim, M.; Schmitt, S. K.; Choi, J. W.; Krutty, J. D.; Gopalan, P. From Self-Assembled Monolayers to Coatings: Advances in the Synthesis and Nanobio Applications of Polymer Brushes. *Polymers (Basel).* **2015**, *7* (7), 1346–1378. https://doi.org/10.3390/polym7071346.

(9) de vos, W. M.; Meijer, G.; de Keizer, A.; Cohen stuart, M. A.; Mieke Kleijn, J. Charge-Driven and Reversible Assembly of Ultra-Dense Polymer Brushes: Formation and Antifouling Properties of a Zipper Brush. *Soft Matter* **2010**, *6*, 2499–2507.

(10) Perrier, S. 50th Anniversary Perspective: RAFT Polymerization - A User Guide. *Macromolecules* **2017**, *50* (19), 7433–7447. https://doi.org/10.1021/acs.macromol.7b00767.

(11) Bingyi, L. I.; Shi, Y.; Zhu, W.; Zhifeng, F. U.; Yang, W. Synthesis of Amphiphilic Polystyrene-b-Poly(Acrylic Acid) Diblock Copolymers by Iodide-Mediated Radical Polymerization. *Polym. J.* **2006**, *38* (4), 387–394. https://doi.org/10.1295/polymj.38.387.

(12) Chen, D.; Fu, Z.; Shi, Y. Synthesis of Amphiphilic Diblock Copolymers by DPE Method. *Polym. Bull.* **2008**, *60* (2–3), 259–269. https://doi.org/10.1007/s00289-007-0873-7.

(13) Greene, A. C.; Zhu, J.; Pochan, D. J.; Jia, X.; Kiick, K. L. Poly(Acrylic Acid-b-Styrene) Amphiphilic Multiblock Copolymers as Building Blocks for the Assembly of Discrete Nanoparticles. *Macromolecules* **2011**, *44*, 1942–1951.

(14) Lu, C.; Chen, L.; Huang, K.; Wang, G. Synthesis and Characterization of Amphiphilic Triblock Copolymers with Identical Compositions but Different Block Sequences. *RSC Adv.* **2014**, *4* (82), 43682–43690. https://doi.org/10.1039/c4ra07084d.

(15) Arcana, M.; Nagesh, K.; Ramakrisnan, S. Synthesis of Narrow Polydispersity Block Copolymers

of PtBA-PS by Novel RAFT Polymerization Technique. *ITB J. Eng. Sci.* **2004**, *36* (1), 63–79. https://doi.org/10.5614/itbj.eng.sci.2004.36.1.5.

(16) Li, L.; Jiang, R.; Chen, J.; Wang, M.; Ge, X. In Situ Synthesis and Self-Reinforcement of Polymeric Composite Hydrogel Based on Particulate Macro-RAFT Agents. *RSC Adv.* **2017**, *7* (3), 1513–1519. https://doi.org/10.1039/c6ra25929d.

(17) Obata, M.; Tanaka, S.; Mizukoshi, H.; Ishihara, E.; Takahashi, M.; Hirohara, S. RAFT Synthesis of Polystyrene-Block-Poly(Polyethylene Glycol Monomethyl Ether Acrylate) for Zinc Phthalocyanine-Loaded Polymeric Micelles as Photodynamic Therapy Photosensitizers. *J. Polym. Sci. Part A Polym. Chem.* **2018**, *56* (5), 560–570. https://doi.org/10.1002/pola.28929.

(18) Chong, B. Y. K.; Le, T. P. T.; Moad, G.; Rizzardo, E.; Thang, S. H. More Versatile Route to Block Copolymers and Other Polymers of Complex Architecture by Living Radical Polymerization: The RAFT Process. *Macromolecules* **1999**, *32* (6), 2071–2074. https://doi.org/10.1021/ma981472p.

(19) Ponnusamy, K.; Babu, R. P.; Dhamodharan, R. Synthesis of Block and Graft Copolymers of Styrene by Raft Polymerization, Using Dodecyl-Based Trithiocarbonates as Initiators and Chain Transfer Agents. *J. Polym. Sci. Part A Polym. Chem.* **2013**, *51* (5), 1066–1078. https://doi.org/10.1002/pola.26466.

(20) Tan, M.; Shi, Y.; Fu, Z.; Yang, W. In Situ Synthesis of Diblock Copolymer Nano-Assemblies via Dispersion RAFT Polymerization Induced Self-Assembly and Ag/Copolymer Composite Nanoparticles Thereof. *Polym. Chem.* **2018**, *9* (9), 1082–1094. https://doi.org/10.1039/c7py01905j.

(21) Cao, Y.; Shi, Y.; Wu, X.; Zhang, L. Preparation of ABA Triblock Copolymer Assemblies through "One-Pot" RAFT PISA. *Chinese Chem. Lett.* **2020**, *31* (6), 1660–1664. https://doi.org/10.1016/j.cclet.2019.10.026.

(22) Jin, C.; Liu, C.; Jiang, B.; Yin, Q. J. Synthesis and Characterization of High Molecular Weight and Low Dispersity Polystyrene Homopolymers by RAFT Polymerization. *E-Polymers* **2012**, No. 035, 1–10. https://doi.org/10.1515/epoly.2012.12.1.418.

(23) Benoit, D.; Chaplinski, V.; Braslau, R.; Hawker, C. J. Development of a Universal Alkoxyamine for "living" Free Radical Polymerizations. *J. Am. Chem. Soc.* **1999**, *121* (16), 3904–3920. https://doi.org/10.1021/ja984013c.

(24) Hamley, I. *Block Copolymers in Solution : Fundamentals and Applications Block Copolymers in Solution : Fundamentals and Applications*; John Wiley & Sons, Ltd, 2005.

(25) Willcock, H.; O'Reilly, R. K. End Group Removal and Modification of RAFT Polymers. *Polym. Chem.* **2010**, *1* (2), 149–157. https://doi.org/10.1039/b9py00340a.

(26) Keddie, D. J.; Moad, G.; Rizzardo, E.; Thang, S. H. RAFT Agent Design and Synthesis. *Macromolecules* **2012**, *45* (13), 5321–5342. https://doi.org/10.1021/ma300410v.

(27) Graeme Moad,* Ezio Rizzardo, S. H. T. End-Functional Polymers, Thiocarbonylthio-Group Removal/Transformation and RAFT Polymerization. *Macromolecules* **2007**, 1796–1798.

(28) Mattson, K. M.; Pester, C. W.; Gutekunst, W. R.; Hsueh, A. T.; Discekici, E. H.; Luo, Y.; Schmidt, B. V. K. J.; McGrath, A. J.; Clark, P. G.; Hawker, C. J. Metal-Free Removal of Polymer Chain Ends Using Light. *Macromolecules* **2016**, *49* (21), 8162–8166. https://doi.org/10.1021/acs.macromol.6b01894.

(29) Carmean, R. N.; Figg, C. A.; Scheutz, G. M.; Kubo, T.; Sumerlin, B. S. Catalyst-Free

Photoinduced End-Group Removal of Thiocarbonylthio Functionality. *ACS Macro Lett.* **2017**, *6* (2), 185–189. https://doi.org/10.1021/acsmacrolett.7b00038.

(30) Jesson, C. P.; Pearce, C. M.; Simon, H.; Werner, A.; Cunningham, V. J.; Lovett, J. R.; Smallridge, M. J.; Warren, N. J.; Armes, S. P. H2O2 Enables Convenient Removal of RAFT End-Groups from Block Copolymer Nano-Objects Prepared via Polymerization-Induced Self- Assembly in Water. *Macromolecules* **2017**, *50* (1), 182–191. https://doi.org/10.1021/acs.macromol.6b01963.

(31) Discekici, E. H.; Shankel, S. L.; Anastasaki, A.; Oschmann, B.; Lee, I. H.; Niu, J.; McGrath, A. J.; Clark, P. G.; Laitar, D. S.; De Alaniz, J. R.; Hawker, C. J.; Lunn, D. J. Dual-Pathway Chain-End Modification of RAFT Polymers Using Visible Light and Metal-Free Conditions. *Chem. Commun.* **2017**, *53* (11), 1888–1891. https://doi.org/10.1039/c6cc08370f.

(32) Discekici, E. H.; Shankel, S. L.; Anastasaki, A.; Oschmann, B.; Lee, I. H.; Niu, J.; McGrath, A. J.; Clark, P. G.; Laitar, D. S.; De Alaniz, J. R.; Hawker, C. J.; Lunn, D. J. Dual-Pathway Chain-End Modification of RAFT Polymers Using Visible Light and Metal-Free Conditions. *Chem. Commun.* **2017**, *53* (11), 1888–1891. https://doi.org/10.1039/c6cc08370f.

(33) Filippov, A. D.; Van Hees, I. A.; Fokkink, R.; Voets, I. K.; Kamperman, M. Rapid and Quantitative De- Tert-Butylation for Poly(Acrylic Acid) Block Copolymers and Influence on Relaxation of Thermoassociated Transient Networks. *Macromolecules* **2018**, *51* (20), 8316–8323. https://doi.org/10.1021/acs.macromol.8b01440.

(34) Xu, Z.; Zhang, C.; Jiao, N. Supporting Information Synthesis of Oxazoles. *Angew. Chem. Int. Ed. Engl.* **2012**, *26* (2), 1–29.

(35) Zhang, S. S.; Cui, K.; Huang, J.; Zhao, Q. L.; Cao, S. K.; Ma, Z. Synthesis of Diverse α,ω-Telechelic Polystyrenes with Di- and Tri-Functionality via Tandem or One-Pot Strategies Combining Aminolysis of RAFT-Polystyrene and a Thiol-Ene “Click” Reaction. *RSC Adv.* **2015**, *5* (55), 44571–44577. https://doi.org/10.1039/c5ra06956d.

7 Appendix

7.1 NMR data polystyrene

7.1.1 IR006 T0 – PS at time 0

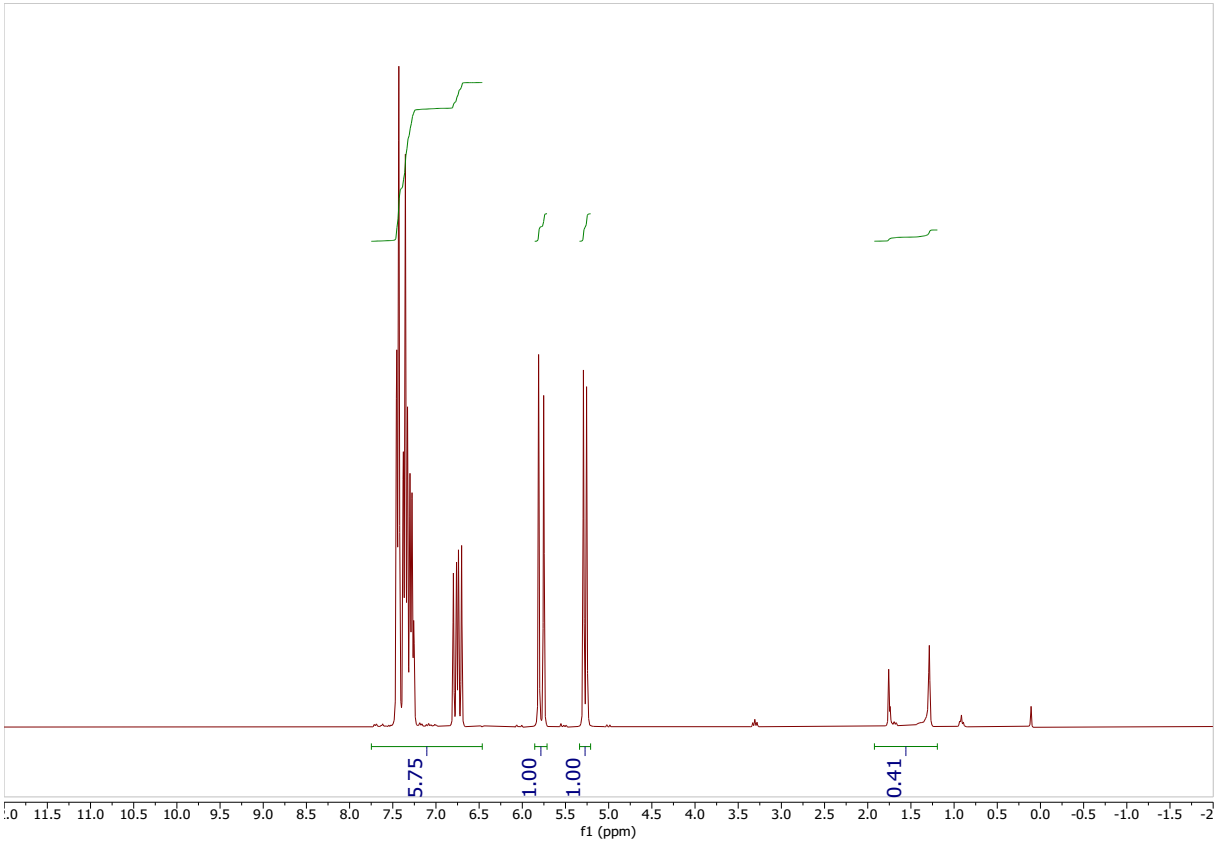

7.1.2 IR006 F – PS when finished after 7 hours

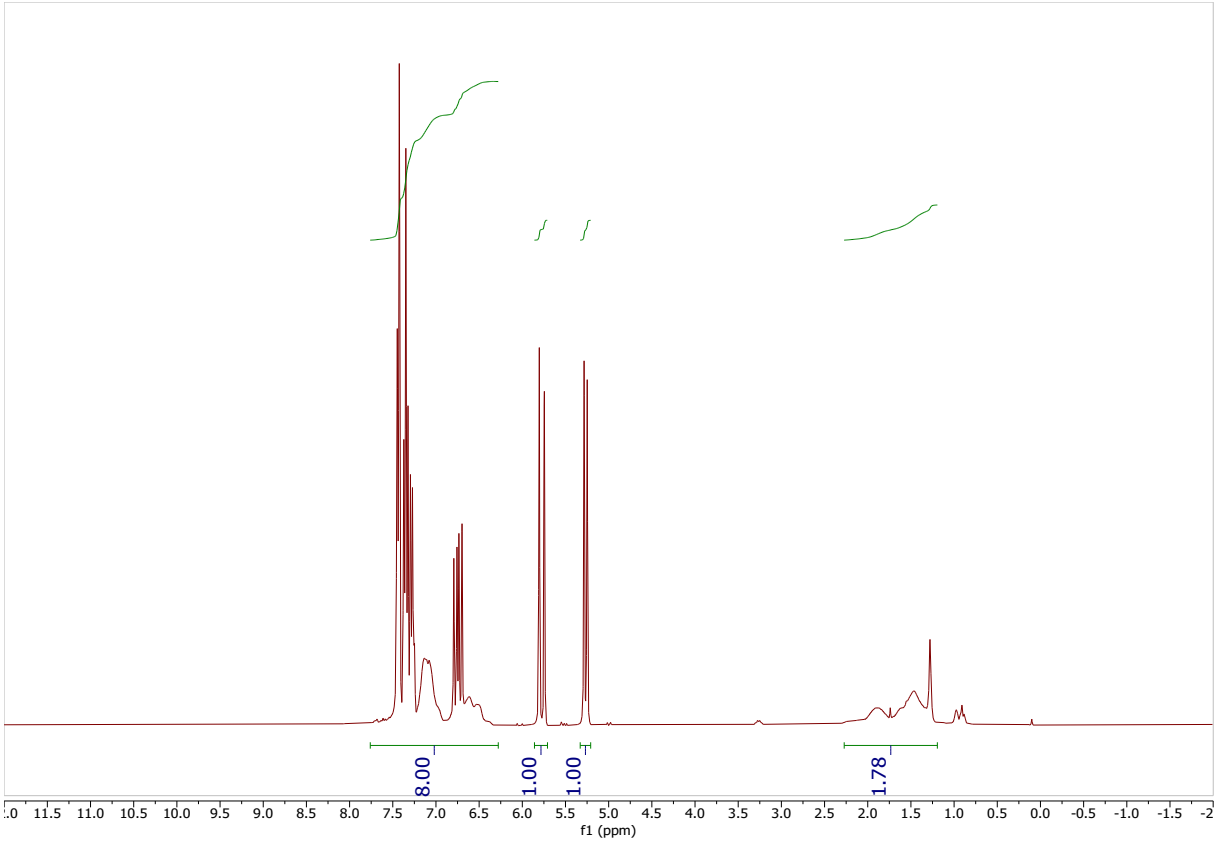

7.1.3 IR018 – PS without CTA

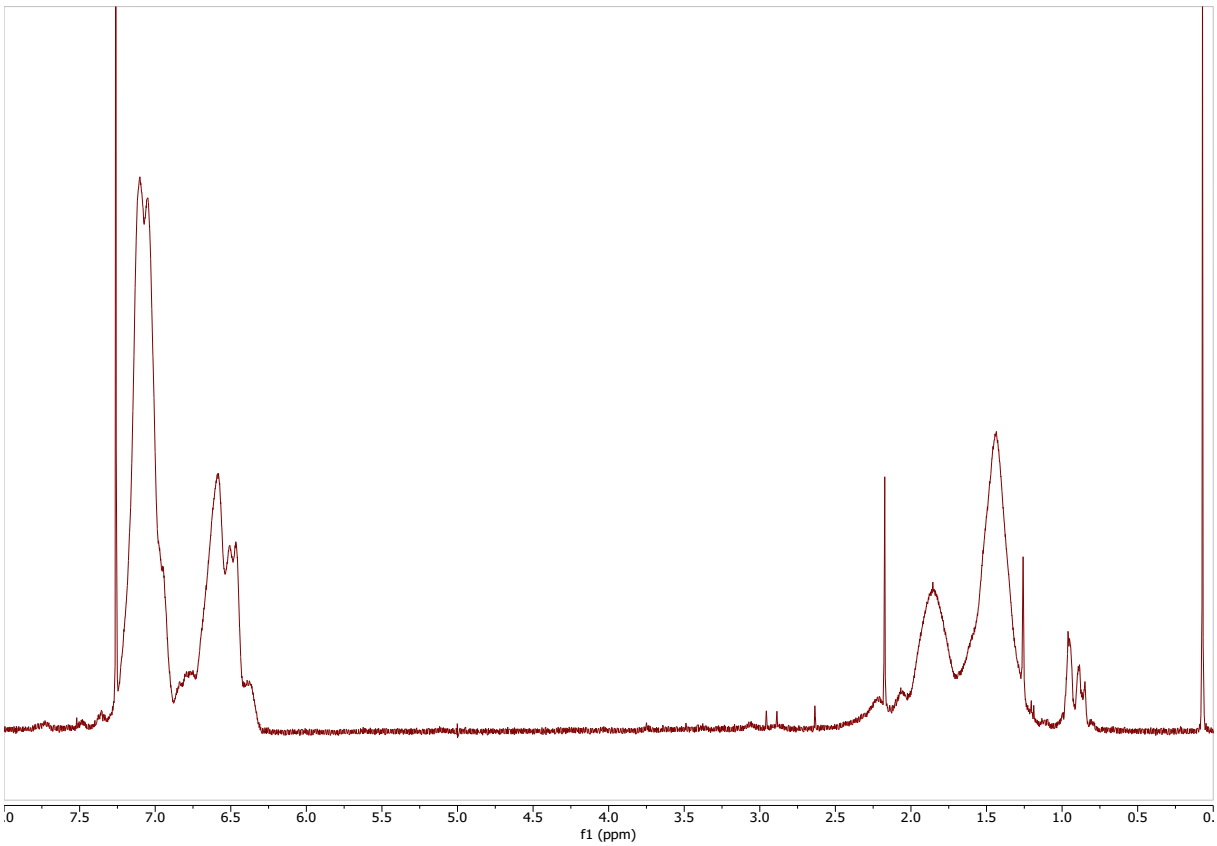

7.1.4 IR024 – Typical PS-*b*-PAA NMR spectra

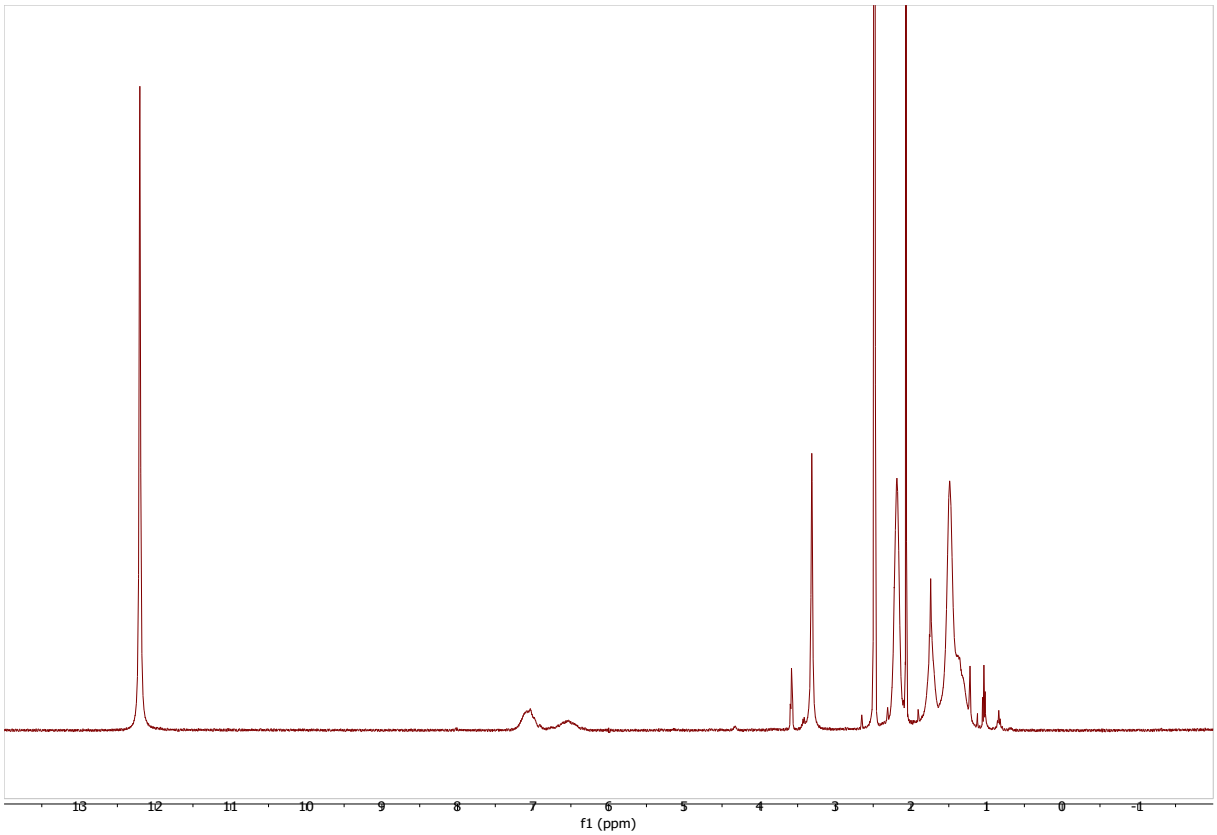

7.1.5 Correlation curve of the DLS